RSC Advances

REVIEW

View Article Online
View Journal | View Issue

Check for updates

Cite this: *RSC Adv.*, 2020, **10**, 33227

Silk fibroins in multiscale dimensions for diverse applications

Pramod Dorishetty, Naba K. Dutta * and Namita Roy Choudhury *

Silk biomaterials in different forms such as particles, coatings and their assemblies, represent unique type of materials in multiple scales and dimensions. Herein, we provide an overview of multi-scale silk fibroin materials including silk particles, silk coatings and silk assemblies, each of which represents a unique type of material with wide range of applications. They feature tunable structures and mechanical properties with excellent biocompatibility, which are essentially required for various biomedical and drug delivery applications. The review focuses on bringing a new perspective on the utilization of regenerated silk fibroins in modern biomedicine by beginning with the fabrication of silk in multiscale dimensions and their state-of-the-art applications in various biomedical and bioelectronic fields. It covers the fundamentals of processing silk fibroins in multi-dimensions (sizes and shapes) with a specific emphasis on its structural tunability at various length scales (nano–micro) by using the latest fabrication methods/mechanisms and advanced fabrication technologies, followed by their recent applications in diverse fields of biomedicine.

Received 2nd May 2020
Accepted 18th August 2020

DOI: 10.1039/d0ra03964k

rsc.li/rsc-advances

Open Access Article. Published on 08 September 2020. Downloaded on 1/22/2026 4:27:21 AM.
This article is licensed under a Creative Commons Attribution-NonCommercial 3.0 Unported Licence.

1 Introduction

The silk fibroin is a natural protein generated by species belonging to phylum *Arthropoda* such as silkworms and spiders.[1] Silk fibroin proteins obtained from different species exhibit slightly varying properties in terms of structure and performance.[2,3] For instance, silk fibroins obtained from different silkworms like *Bombyx mori* and *Antheraea mylitta* exhibit different molecular weights and structural properties.[4,5] In general, the regenerated silk fibroin consists of a series of repetitive amino acid sequences (primary structure), which rearrange into secondary structures *via* hydrogen bonding, hydrophobic interactions and di-sulfide bonds, thereby influencing the overall characteristics of the silk construct.[6] The silk fibroin engineered by *Bombyx mori* is highly biocompatible and comprises hydrophobic heavy chains (H-fibroin, M_w = 391.6 kDa) and hydrophilic light chains (L-chain, M_w = 27.7 kDa) linked by a single disulfide bond at the C-terminus.[7,8] The heavy hydrophobic chain mainly consists of the hexapeptide sequence GAGAGS, which undergoes structural transformation due to strong hydrogen bonding and hydrophobic interactions forming heavy crystalline fractions (alanine or glycine rich sequences) and interspersed amorphous regions (less

School of Engineering, RMIT University, Melbourne, Victoria 3000, Australia. E-mail: namita.choudhury@rmit.edu.au

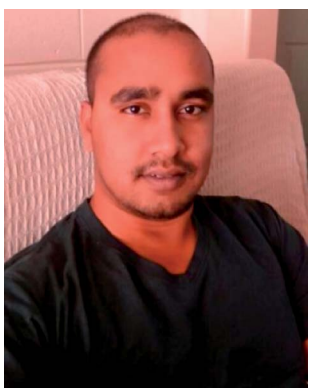

Pramod Dorishetty obtained his bachelor's (2014) and master's (2016) degree in Chemical Engineering from Osmania University and IIT Madras, India, respectively. Currently, he is completing his PhD at the School of Engineering, RMIT University, Australia. His research interests include engineering tough hydrogels from protein polymers to mimic natural tissue analogues and development of protein inks for 3D printing complex architectures for load bearing tissue engineering applications.

Naba K. Dutta is currently a Professor at the Chemical & Environmental Engineering Discipline of RMIT University. Upon receiving his PhD from IIT, Kgp, and post-doctoral research in France, he joined Monash University and later the University of South Australia. His research interest is in nanomaterials, nanobioconjugates and smart biopolymers for catalytic and biomedical applications.

Open Access Article. Published on 08 September 2020. Downloaded on 1/22/2026 4:27:21 AM.
This article is licensed under a Creative Commons Attribution-NonCommercial 3.0 Unported Licence.

organized amino acids), resulting in remarkable strength and elasticity.[9–11] Moreover, the degradation rate of the silk construct can be tailored from days to months by employing different strategies such as varying molecular weight, crystalline fraction, crosslinking degree, and amalgamation with other polymers.[12,13] In addition to biocompatibility, silk fibroins also offer flexibility in processing to achieve tunable structures and properties. The scaled-up and reliable fabrication and assembly of silk biomaterials are, therefore, a prerequisite for the development of silk-based biomedical systems and devices. It all started in the 1930s when the German and Japanese scientists successfully patented the dissolution of silk fibers to make a silk fibroin feedstock and later used it to construct various formats.[14] The capability to process silk fibroins into multiscale dimensions such as particles/crystals, fibers, films and 3D porous hydrogels with tunable characteristics thrived its utilization in various applications in modern biomedicine. Fig. 1 shows the scope of this review. For easy portraying, crystals, fibers, films or gels fabricated from a silk fibroin solution are simply referred to as silk fibroin constructs in the rest of the manuscript. The fabrication/processing of silk fibroins in multiscale dimensions greatly influences their overall characteristics to determine their application in various fields.[15] For example, silk particles (nano–micro) are vastly used in drug delivery applications, whereas silk films find applications in wound healing and biocompatible coatings and 3D silk hydrogels are primarily used in tissue scaffolds and controlled drug release applications.[16]

Apart from physiochemical characteristics and tunability, silk fibroin constructs also show the capability to tailor biological characteristics such as adhesion, proliferation and differentiation by tuning the cell–surface interactions.[27] The cell–surface interactions greatly depend on the biomaterial surface's physicochemical properties, such as the availability of integrin recognition sequence, surface wettability, hydrophobicity/hydrophilicity and surface stiffness. A detailed review of the effect of surface characteristics of silk fibroin constructs on cellular response is discussed elsewhere.[28] Due to the outstanding properties including biocompatibility, tunable structural, mechanical and biological properties of silk fibroins, they have been explored in diverse fields of healthcare with successful clinical trials.[14] The control over the tunability of the silk fibroin architecture in different formats is so far primarily driven by specific processing conditions (process-driven); whereas, the recent advanced fabrication approaches such as lithography and 3D printing are design-driven fabrication methods, which made it possible to control the architecture of the fabricated silk constructs at micro–nano-scale resolutions.[29] The control over the fabrication of silk constructs with nano–micro resolution and the ability to incorporate conducting materials opened a new window for the use of silk fibroins in bioelectronic devices, efficient drug carrying devices and neural tissue engineering. There are numerous reviews on silk biomaterials in terms of structures, processing, composites and applications.[30–32] However, in this review, we present an in-depth understanding and fundamentals of processing silk fibroins with tunable properties in multiscale dimensions with specific emphasis on the use of latest and advanced fabrication approaches to augment their use in diverse biomedical applications (Fig. 2).

Namita Roy Choudhury is a Professor at the School of Engineering, RMIT University. She received her PhD from IIT, Kharagpur and subsequently did her post-doctoral research at CNRS, Mulhouse, France. Choudhury's research interest spans from hydrogels to biomimetic polymers to printable inks for biomedical and advanced manufacturing.

2 Fabrication of silk fibroins in multiscale dimensions

The fabrication or processing of silk fibroins in different dimensions is critical in dictating its overall characteristics and determining the application. In this section, we discuss the fabrication of silk fibroins in multiscale dimensions (Table 1) with specific emphasis on the recent advanced fabrication approaches and the corresponding mechanism involved.

2.1 Silk particles (nano–micro)

Silk fibroin can be processed into particles by various methods such as ball milling, spray drying, phase separation, and solvent precipitation.[33–35] In majority of the studies, authors employed the self-assembly mechanism of silk fibroins by exploiting the micelle-forming capability of their hydrophobic (Gly and Ala) and hydrophilic (Tyr and Ser) segments, as shown in Fig. 3A.[36] Some of the important and facile methods of silk particle fabrication are discussed below.

2.1.1 Phase separation process. Phase separation is the most commonly employed mechanism to separate water-soluble protein particles by introducing external organic solvents. The increase in organic solvents decreases the solubility of the protein and separates the protein molecules by phase separation.[37] Many organic solvents such as ethanol, methanol, propanol and isopropanol were explored in separating the silk protein particles of various sizes (nm–μm).[35] For example, the simple addition of ethanol to dilute the silk fibroin solution resulted in silk particles of 2.7 μm diameter.[38] The obtained microparticles are highly sustainable and useful in the delivery of bone morphogenetic protein (BMP) in tissue engineering applications (Fig. 3C). In other study, ethyl acetate is used as an organic solvent to make silk particles, wherein the silk fibroin solution was added to ethyl acetate, followed by the separation of the particles by centrifugation (Fig. 3B).[39] The obtained silk particles are in the size range of 23–67 μm, which

 This journal is © The Royal Society of Chemistry 2020

Open Access Article. Published on 08 September 2020. Downloaded on 1/22/2026 4:27:21 AM.
This article is licensed under a Creative Commons Attribution-NonCommercial 3.0 Unported Licence.

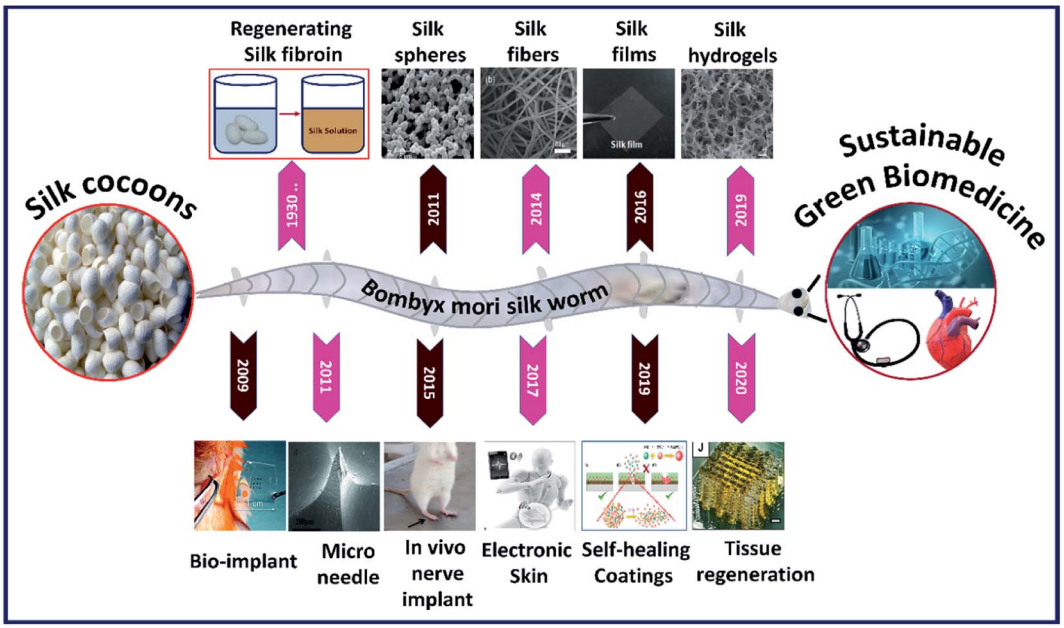

Fig. 1 Images of silk fibroins fabricated in multiscale dimensions (in the last decade) such as microparticles. Reprinted with permission from ref. 17 Copyright © 2011 Elsevier. Fibers. Reprinted with permission from ref. 18 Copyright © 2014 Royal Society of Chemistry. Films. Reprinted with permission from ref. 19 Copyright © 2016 Wiley. Hydrogel cross-sectional morphology. Reprinted with permission from ref. 20 Copyright © 2019 Elsevier. And the timeline representing the progression of its application in modern biomedicine such as bioimplant. Reprinted with permission from ref. 21 Copyright © 2009 AIP Publishing. Microneedle. Reprinted with permission from ref. 22 Copyright © 2011 Wiley. Nerve implant. Reprinted with permission from ref. 23 Copyright © 2015 Elsevier. Electronic skin. Reproduced with permission from ref. 24 Copyright © 2017 Wiley. Self-healing coatings. Reproduced with permission from ref. 25 Copyright © 2019 Elsevier and Tissue regeneration. Reprinted with permission from ref. 26 Copyright © 2020 Wiley.

Fig. 2 Graphical illustration of combining advantages of silk fibroins in multiscale dimensions with advanced technologies to augment their use in various fields of biomedicine.

are suitable as microcarriers for hydrophilic drug delivery. The addition of potassium phosphate to an aqueous silk fibroin solution also triggers the silk particle formation by inducing phase separation.[40] The size of silk particles was tuned between 0.48 and 2 μm by manipulating the silk fibroin concentration, and these silk particles are successfully used as controlled drug delivery devices. The silk particles at nanoscales can also be obtained by exploiting the spontaneous micro-phase separation between silk fibroin and polyvinyl alcohol (PVA) (Fig. 3D).[17,41] The nanoscale silk particles are obtained by dissolving silk/PVA films in pure water, followed by centrifugation at a high speed of 16 000 rpm and resuspending them in water by sonication.[42] The obtained silk spheres are in nanoscale ranging from 100 to 500 nm, which found applications in drug delivery. Recently, Takeuchi *et al.* have used acetone as a solvent to make silk particles of size 40 nm.[43] The very small size of silk particles favored in the successful transdermal delivery of drugs by penetrating the stratum corneum and reaching hair follicles in mice.

2.1.2 Advanced jetting process. In addition to phase separation and molecular self-assembly, silk particles can also be prepared by an advanced fabrication process. For example, silk microspheres are fabricated physically by precisely slicing a thin silk fibroin solution jet by vibrating the nozzle at a controlled frequency and amplitude.[45] The produced spheres (100–440 μm) were collected and shock frozen in a liquid nitrogen bath and freeze-dried for drug delivery applications (Fig. 4A). Moreover, the spheres size can be controlled or tuned by adjusting the nozzle diameter. Silk fibroin nano spheres are also fabricated using a microfluidic device (co-flow capillary) by exploiting the phase separation mechanism using PVA.[46] Silk spheres are formed by breaking off the discrete phase silk fibroin in the continuous phase of PVA (Fig. 4B). Using this method, the size of the spheres can be tuned form 210 nm to

Open Access Article. Published on 08 September 2020. Downloaded on 1/22/2026 4:27:21 AM. This article is licensed under a Creative Commons Attribution-NonCommercial 3.0 Unported Licence.

Table 1 Fabrication/processing of silk fibroins in multiscale dimensions and their applications

Multiscale silk	Mechanism/fabrication	Applications	Ref.
Silk nanoparticles	Phase separation using PVA	Drug delivery	17
Silk microparticles	Ethanol addition to silk fibroin solution	Protein carrier	38
Silk microspheres	Water in oil emulsion solvent diffusion	Drug delivery	39
Silk microparticles	Addition of potassium phosphate to silk fibroin solution	Drug delivery	40
Silk microspheres	Phase separation using PVA	Drug delivery	42
Silk nanoparticles	Adding silk fibroin solution to acetone solvent.	Drug delivery	43
Silk microspheres	Physical formation/laminar jet breakup	Drug delivery	45
Silk microspheres	Phase separation using PVA and using co-flow capillary device.	Drug delivery	46
Silk nanoparticles	Ball milling of silk membrane	Wound healing	74
Silk microspheres	Spray-drying	Fundamental study	75
Silk films (2D)	Solution cast drying	Fundamental study	50
Silk films (2D)	Spin coating and spin-assisted layer-by-layer assembly	Biomedical devices	47
Silk films (2D)	Spin coating & electro-spinning followed by ethanol treatment	Fundamental study	48
Silk films (2D)	Spin coating & soft lithographic technique	Fundamental study	52
Silk films (2D)	Centrifugal casting	Corneal tissue engineering	19
Silk micropatterns (2D)	Spin coating & photolithography	Fundamental study	53
Silk nano–micro patterns (2D)	Soft lithography & casting	Bio-optics	54
Silk films (2D)	Spin coating & nanoimprinting	Bio-photonics	55
Silk films (2D)	Electro gelation	Fundamental study	51
Silk e-gel (3D)	Electro gelation	Fundamental study	60
Silk scaffold (3D)	Freeze-drying	Tissue engineering	61
Silk hydrogel (3D)	Photo-crosslinking	Tissue engineering	62
Silk scaffold (3D)	3D printing and ethanol treatment	Tissue engineering	71
Silk/HPMC scaffold (3D)	3D printing microgel and ethanol treatment	Tissue engineering	72
Silk-Ma scaffolds (3D)	3D printing and photo-crosslinking	Tissue engineering	73
Silk hydrogel (3D)	3D printing and photo-crosslinking	Tissue engineering	26

2000 nm by adjusting the flow rate and changing the concentration of silk fibroin and PVA. The tunable micro- and nanospheres found applications in the delivery of drugs and contrast agents for noninvasive sensing.

2.2 Silk films (2-dimensional)

Silk fibroin films are generally fabricated by casting, spin coating, electrospinning and a layer-by-layer assembly method.[32,47,48] During film formation, the silk fibroin solution transforms from silk I to silk II structure found applications in wound healing, bioelectronics, coatings, *etc.* Some of the important approaches for fabricating silk films are discussed below.

2.2.1 Solution casting. The most commonly employed silk film fabrication approach is casting a dilute silk fibroin solution and subsequent drying.[49] Simply, a silk fibroin solution is casted on a glass slide or a coverslip and subsequently dried overnight to get a thin film. However, these films are transparent with a fast degradation rate and mechanically unstable. The stability of these films can be improved by alcohol treatment (methanol and ethanol) and water annealing, where the conformational change of silk I to silk II (β-sheet) structure occurs.[32] The conversion of silk I to silk II structure can be controlled by different methods like adjusting the concentration, processing temperature and the rate of drying process.[50] Apart from general casting under the influence of gravitation, ultrafine silk films (thickness 50 μm) can also be fabricated by subjecting the silk fibroin solution to centrifugal force (Fig. 5A).[19] The films fabricated using centrifugal force demonstrated excellent toughness, less surface roughness and better cytocompatibility when compared to the films made by casting and suitable for corneal tissue engineering applications. The general casting process requires solvent drying to induce crystallization, which takes several hours (12–36 hours) to get the final product, hindering the mass production of devices. Electro-gelation is a novel approach to form transparent silk films with a controlled architecture in ~30 minutes.[51] The silk fibroin aggregates around the anode and forms a thin film when subjected to electrical stimulations. By adjusting the shape of the anode, the silk films with different structures like circular, s-shaped and saddle point and tubular geometries can be made, which is highly challenging to fabricate by conventional approaches like casting or coating (Fig. 5B).

2.2.2 Advanced fabrication approach. Although researchers' fabricated thin silk films by exploiting different approaches (casting, centrifugal force, and electro-gelation); with the increase in interdisciplinary research, there has been a growing interest in the field of bioelectronics and biosensing, which requires control of the 2D architecture over different length scales (nano–micro). By exploiting the recent advanced technology, a novel strategy is reported in which the secondary structure of the silk fibroin is controlled by micropatterning using a soft lithographic technique with high spatial resolution.[52] Briefly, the spin-coated silk I film is masked with polystyrene (PS) and exposed to ethanol vapor, which turned the exposed silk I structure to a highly stable silk II structure. Later, the PS mask is dissolved using toluene leaving a silk film with

 This journal is © The Royal Society of Chemistry 2020

Open Access Article. Published on 08 September 2020. Downloaded on 1/22/2026 4:27:21 AM.
This article is licensed under a Creative Commons Attribution-NonCommercial 3.0 Unported Licence.

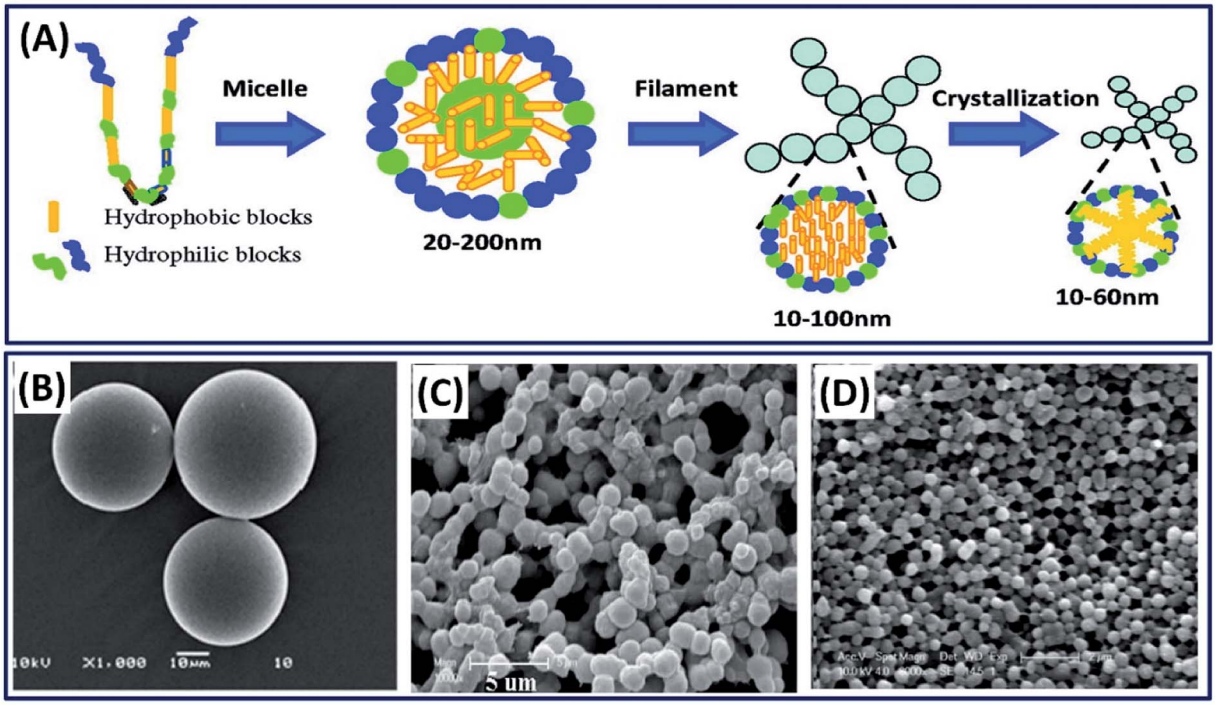

Fig. 3 (A) Schematic of silk fibroin assembly mechanism. Reproduced with permission from ref. 44 Copyright © 2012 American Chemical Society. SEM micrographs of silk fibroin particles fabricated by (B) emulsion solvent diffusion method. Reprinted with permission from ref. 39 Copyright © 2010 Elsevier. (C) Ethanol precipitation method. Reprinted with permission from ref. 38 Copyright © 2010 Wiley. (D) Phase separation with polyvinyl alcohol (PVA). Reprinted with permission from ref. 17 Copyright © 2011 Elsevier.

gradient silk I and silk II structures (Fig. 6A). The micro-patterned silk I and silk II films demonstrated excellent gradient properties and found applications where uniform surface chemistry and variable (gradient) mechanical properties are required.

Silk fibroin has also been used in conjugation with photolithography to form 2-dimensional architectures at micro- and nanoscales with excellent resolution and shape fidelity.[53] In such process, a photomask with micro/nanopatterns is covered on the spin-coated substrate and the light-exposed regions are turned into micro and nanopatterns. The ability to precisely pattern silk fibroins at such small scales can widen their use in microelectronics. Mechanically robust and optically transparent silk films with micro- and nanopatterns made by the soft-lithography casting process have been reported for bio-optics applications.[54] In a study by Amsden *et al.*, the authors made silk films using a rapid nano-imprinting approach at room temperature, in which a nanoscale master pattern is pressed onto the spin-coated silk film on a glass slide (Fig. 6B(a)).[55] The 2-dimensional inexpensive silk films with nano resolution (Fig. 6B(b)) showed the excellent capability of

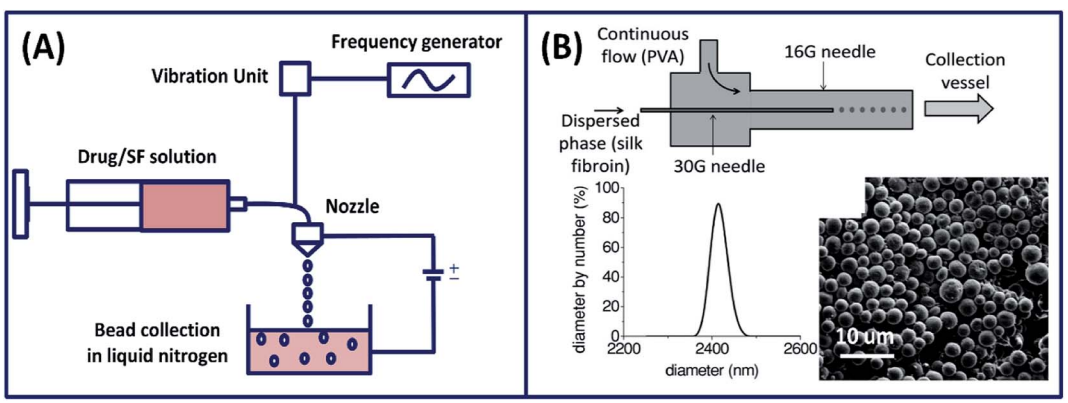

Fig. 4 (A) Illustration showing the experimental setup used for the preparation of silk fibroin spheres by laminar jet breaking. Reprinted with permission from ref. 45 Copyright © 2008 Elsevier. (B) A schematic of the silk particle fabricated by a co-flow capillary device with particle size distribution (using DLS) and SEM image of dried silk microspheres. Reprinted with permission from ref. 46 Copyright © 2013 Wiley.

Open Access Article. Published on 08 September 2020. Downloaded on 1/22/2026 4:27:21 AM.
This article is licensed under a Creative Commons Attribution-NonCommercial 3.0 Unported Licence.

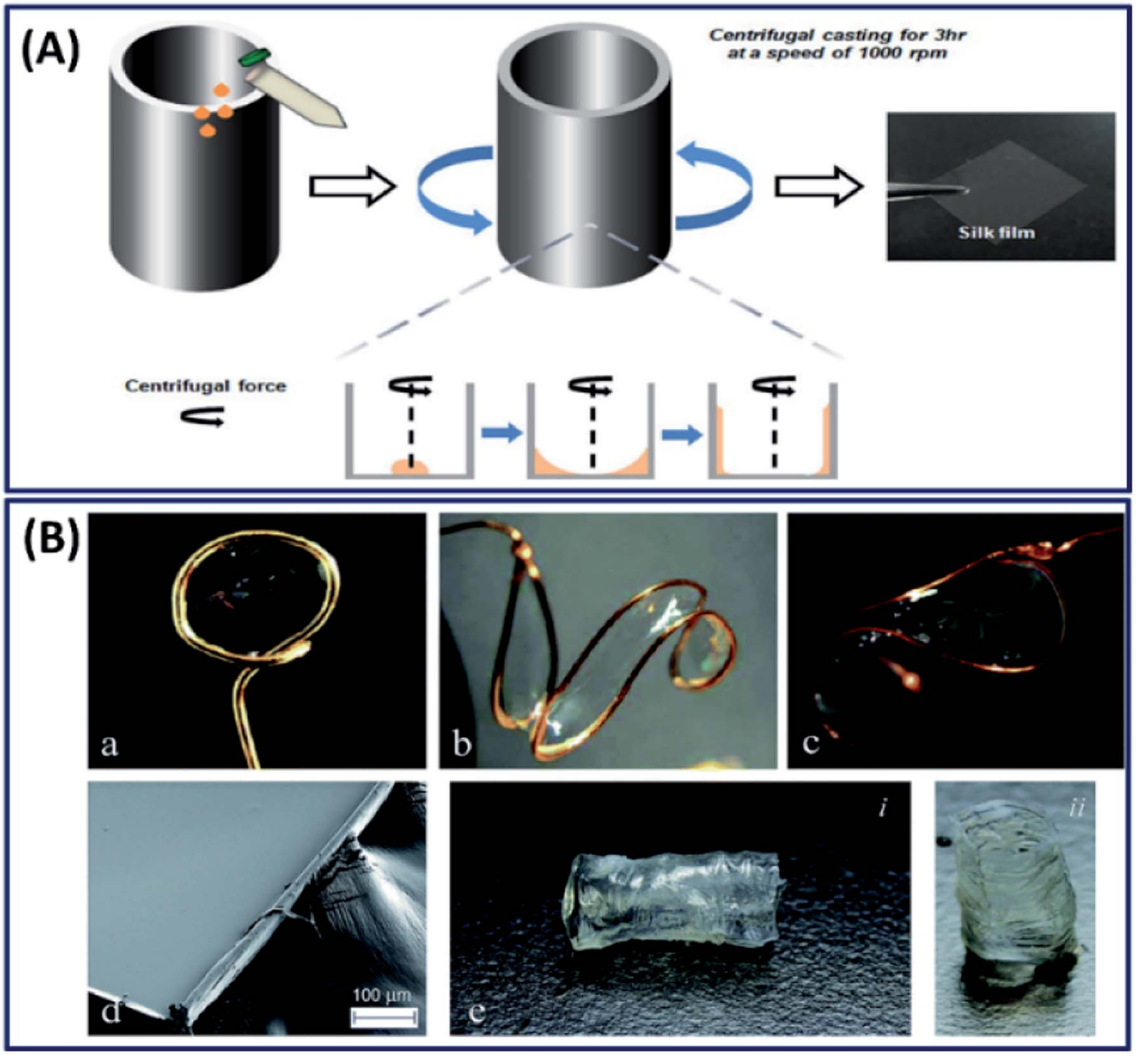

Fig. 5 (A) Schematic of the silk fibroin film fabrication process with the aid of centrifugal force. Reprinted with permission from ref. 19 Copyright © 2016 Wiley. (B) Selection of anode geometries reflects the ability of this process to create silk films with varying non-planar topologies. Anode geometries include: (a) ring, (b) 'S'-shape, and (c) saddle point. (d) SEM image of an e-gel film segment, illustrating gross smoothness of the e-gel film face across a larger area. The edge roughness is due to manual cutting with a razor blade. (e) Tubular e-gel obtained by using a rod-shaped anode. Reproduced with permission from ref. 51 Copyright © 2014 Royal Society of Chemistry.

sensing oxygen binding to hemoglobin, demonstrating its suitability for biophotonics applications.

2.3 Fabrication of silk hydrogels/scaffolds (3-dimensional)

Fabrication of silk hydrogels/scaffolds on a 3-dimensional scale is important for tissue engineering applications because the 3D structures mimic the exact physiological environment of natural tissue constructs. Hydrogel scaffolds are the most common form of 3-dimensional silk fibroin, which consist of either physical or chemical crosslinks with interconnecting networks holding large amounts of water.[56]

2.3.1 Conventional approaches. Silk hydrogels from the silk fibroin solution are naturally formed by the physical crosslinking in which the sol–gel transition of silk fibroin occurs by the self-assembly of its hydrophobic protein chains.[57] However, the self-assembly mechanism is driven by the concentration of silk fibroin and usually takes a longer period. To enhance the self-assembly mechanism, several approaches are being used, which include ultra-sonication, vortexing, shearing, changing temperature and pH conditions using salts like $CaCl_2$ or KCl.[57,58] In addition to natural formation, the silk-based hydrogels are made by chemical crosslinking, photo-crosslinking, reswelling after freeze-drying, electro-gelation and 3D printing. The silk hydrogel fabrication process plays an important role in determining the nano-, micro- and hierarchical structure evolution of the 3D construct,[59] for example, the surface morphology of silk hydrogel fabricated by electro-gelation demonstrated particulate morphology.[60] In contrast, the silk hydrogel made by unidirectional freeze-drying results in a lamellar structure,[61] and by chemical photo-crosslinking mechanism shows a porous structure with interconnected pores (Fig. 7).[62] The microstructure tunability of the silk fibroin

Open Access Article. Published on 08 September 2020. Downloaded on 1/22/2026 4:27:21 AM.
This article is licensed under a Creative Commons Attribution-NonCommercial 3.0 Unported Licence.

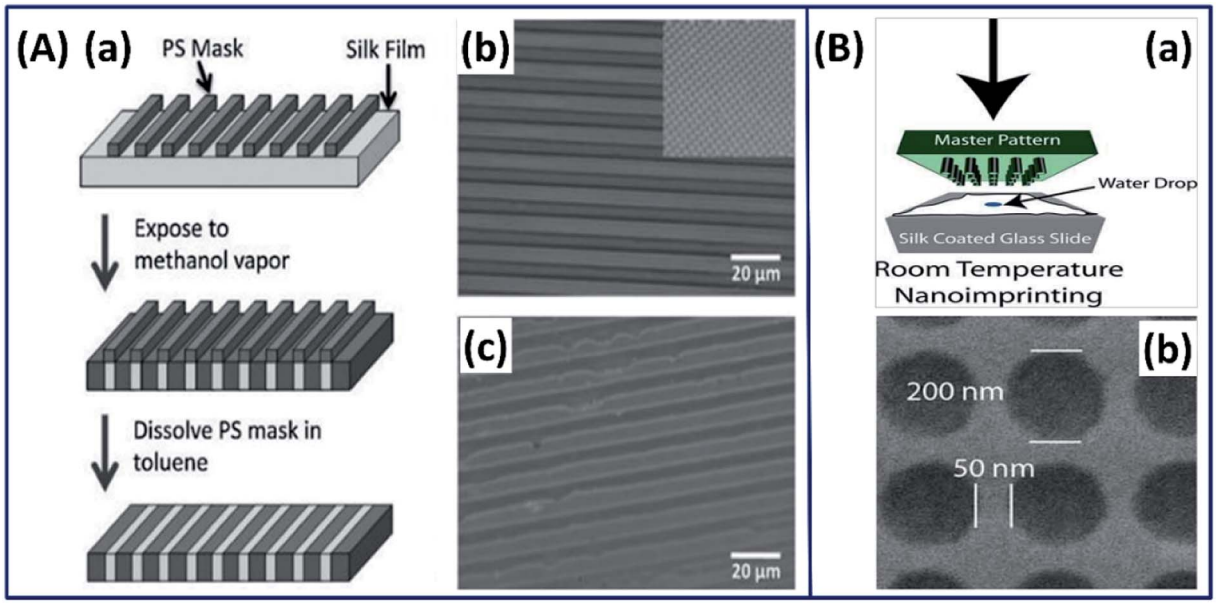

Fig. 6 (A) Strategy for patterning secondary structure in silk films. (a) Schematic of the patterning strategy, from top to bottom (b) optical image of silk film with a PS mask deposited on top. Inset: the square pattern on the same scale. (c) Optical image after removal of the PS mask in toluene. Reprinted with permission from ref. 52 Copyright © 2010 Wiley. (B) 2D nano imprinted silk film. (a) Schematic of nanoimprinting processes at room temperature. (b) SEM image of a silk film imprinted with a periodic array of 200 nm diameter. Reprinted with permission from ref. 55 Copyright © 2010 Wiley.

construct is highly desirable in tissue engineering applications because the interconnected porous structure of the cartilage and lamellar structure of annulus fibers associated with intervertebral disc (IVD) can be easily mimicked by simply adopting the suitable fabrication approach. Besides, silk hydrogels fabricated by photocrosslinking mechanism can be exploited in developing injectable and 3D-printed hydrogels.[63] Recently, we have demonstrated and reported the 3D printability of silk-based hydrogels by exploiting the rapid ruthenium-mediated photo-crosslinking (<1 min) reaction.[62] Moreover, the hydrogels made by this mechanism exhibit tunable structural and mechanical properties with excellent cell attachment and chondrogenic differentiation, demonstrating its suitability for cartilage repair.[64–68]

2.3.2 Advanced fabrication approach (3D printing). Although silk fibroins are fabricated as 3D scaffolds with control over microstructure, mechanical strength, degradation and biological properties to mimic the natural tissue counterparts, the control over reproducibility, cell distribution, and hierarchical architecture is very difficult to accomplish using the conventional fabrication.[69] The advanced fabrication approach such as 3D printing has made it possible to control the architecture from micro- to macro-scale by depositing silk fibroins layer by layer to construct a complex scaffold with holistic control over design and biological properties.[70] Based on the 3D printing approach, a mechanically robust and biocompatible 3D silk scaffold has been made by simply drawing the concentrated silk fibroin solution (25 wt%) in

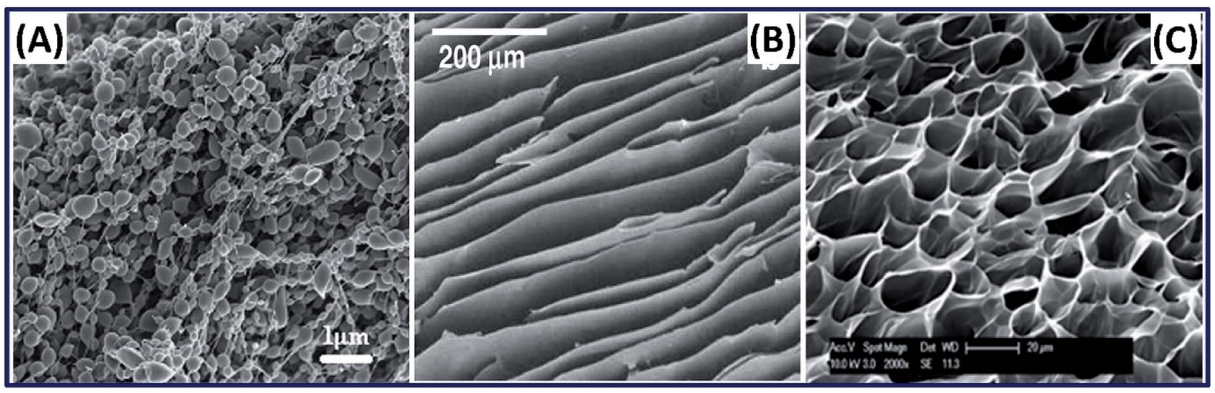

Fig. 7 SEM images of silk 3D hydrogels fabricated by different methods. (A) Electro-gelation (particulate structure). Reprinted with permission from ref. 60 Copyright © 2011 Elsevier. (B) Freeze drying (lamellar structure). Reprinted with permission from ref. 61 Copyright © 2012 Elsevier. (C) Chemical crosslinking (micro porous). Reprinted with permission from ref. 62 Copyright © 2020 American Chemical Society.

Open Access Article. Published on 08 September 2020. Downloaded on 1/22/2026 4:27:21 AM.
This article is licensed under a Creative Commons Attribution-NonCommercial 3.0 Unported Licence.

methanol where the silk fibroin solution transforms to gel state immediately by forming β-sheet upon exposure to methanol (Fig. 8A).[71] The printed scaffold showed excellent structural and mechanical properties along with human bone marrow-derived mesenchymal stem cell (hMSC) adhesion and chondrogenic differentiation, demonstrating its suitability for cartilage tissue engineering applications. Dong *et al.* employed a two-step procedure in which the silk fibroin is combined with hydroxypropyl methylcellulose (HPMC) to form a microgel with excellent thixotropic characteristics.[72] The thixotropic silk fibroin/HPMC is directly printed on a substrate, followed by immersion in ethanol to stabilize it by physical crosslinking (Fig. 8B). The printed construct demonstrated a micro-porous structure with excellent mechanical properties, hMSC compatibility, indicating its use in tissue repair or regeneration.

Silk fibroin is also printed into different complex structures such as ear, brain, heart, and blood vessel with an excellent resolution by functionalizing it with methacrylate (Ma) to form a photocurable Sil-Ma solution (Fig. 9A).[73] The printed structures are mechanically stable, biocompatible and microporous in nature, demonstrating their potential for direct organ printing. The authors functionalized the silk fibroin with methacrylate (Ma) to make it photocrosslinkable. However, using appropriate photoinitiators, silk fibroin alone could be crosslinked from the ink that avoids the additional functionalization of the silk fibroin chain.[64] Based on this mechanism very recently, a cell-encapsulated silk fibroin is printed with high resolution (40 μm) by exploiting di-tyrosine crosslinking formation under visible light.[26] The photo-crosslinked 3D-printed silk hydrogels demonstrated stable mechanical properties and supported long-term chondrocyte culture with cartilage tissue formation, demonstrating the importance of 3D-printed silk scaffolds for potential tissue regeneration applications (Fig. 9B).

3 Applications

The applications of silk fibroins are vastly explored in the fields of drug delivery, wound healing and regenerative medicine in the past. However, the ability of the silk fibroin to transform into a conducting material and to incorporate conducting materials or polymers opened a new platform in neural tissue engineering, in which the neural cells are stimulated/activated using mild electrical signals. Moreover, the control over the 2D architecture with micropatterns with nanoscale resolution and the sensitivity to respond to external stimuli augmented its use in efficient drug delivery, bioelectronics, *etc.* In this section, we discuss the diverse recent applications of silk fibroins in various fields of biomedicine.

3.1 Tissue engineering applications

Tissue engineering is a branch of science that evolved to engineer the human tissue analogues by integrating the expertise from material scientists and cell biologists.[76] The physicochemical characteristics of human tissues are highly complex and vary from soft to rigid and isotropic to anisotropic/gradient structures.[77] For instance, the skin has soft mechanical characteristics, whereas tissues like articular cartilage and the spinal disc are tough and flexible and the human ligaments/tendons are tough with a gradient structure. Engineering those tissue analogues requires a fundamental understanding of the material characteristics in terms of structural, mechanical and biological properties. Owing to the superior biocompatibility and tunable mechanical, structural and degradation characteristics of silk fibroin constructs, it has been explored in various tissue engineering applications as discussed below.

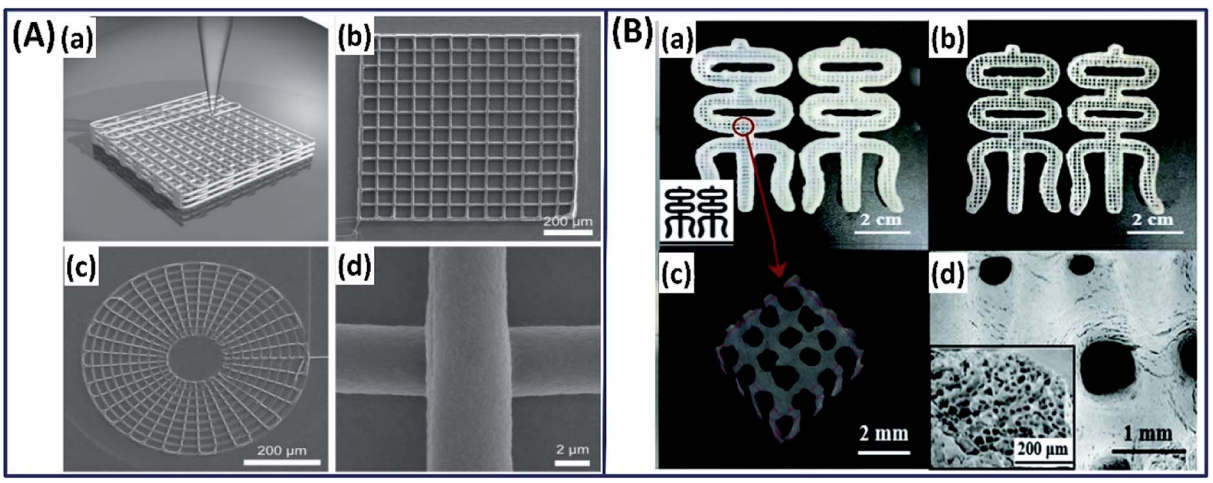

Fig. 8 (A) 3D printing of silk fibroin in methanol reservoir by direct writing. (a) Schematic illustration of 3D structures, (b) square lattice, (c) circular web and (d) magnified image of direct-write silk fiber. Reproduced with permission from ref. 71 Copyright © 2008 Wiley. (B) Images of the 3D-printed (a) RSF hydrogel and (b) RSF lyophilized scaffold in Chinese character "silk". (c) Micro-CT reconstruction of printed RSF hydrogel. (d) FE-SEM image of the printed RSF scaffold. Inset: the porous structure of the scaffold. Reprinted with permission from ref. 72 Copyright © 2019 Royal Society of Chemistry.

 This journal is © The Royal Society of Chemistry 2020

Open Access Article. Published on 08 September 2020. Downloaded on 1/22/2026 4:27:21 AM.
This article is licensed under a Creative Commons Attribution-NonCommercial 3.0 Unported Licence.

3.1.1 Cartilage tissue engineering

Cartilage is a 3-dimensional complex tissue with a porous interconnected structure present between bone joints and acts as a shock absorber providing the frictionless movement of bones.[78] These tissues are highly flexible and mechanically robust at the same time. For example, articular cartilage has a shear modulus of 0.18–2.5 MPa and a healthy human thoracic spinal disc has a compressive modulus of 15–25 MPa.[79–81] Unlike other body tissues, cartilage lacks the self-repairing capability because of its aneural, avascular nature and possesses dense extracellular matrix (EXM).[82] Mimicking the ECM is an important criteria in selecting a biomaterial for cartilage repair, which is satisfied by silk fibroin constructs.[83] The versatility of processing silk fibroin in multiple scales (especially 3D form for cartilage) with interconnected porous structures by employing different fabrication approaches such as freeze-drying, electrospinning, hydrogelation and 3D printing makes it an ideal candidate for the repair of various cartilage damages/diseases.[84] Silk fibroin scaffold fabricated by the freeze-drying process demonstrated interconnecting porous three-dimensional structures with excellent mechanical properties and cartilage matrix formation.[85] Due to the excellent mechanical properties of silk fibroin scaffolds, it is also explored in treating the intervertebral degenerative disc diseases by mimicking the lamellar structure of the spinal disc associated with annulus fibers (AF).[86] In a study by Hu *et al.*, a silk-based injectable 3D hydrogel has been developed for the nucleus pulposus (NP) replacement of the spinal disc using silk fibroins and polyurethane (PU).[87] The resulting hydrogel demonstrated excellent mechanical properties with fatigue resistance and *in vivo* biocompatibility. The implanted silk/PU hydrogel reported being non-toxic with no inflammatory response even after 3 months in the muscle tissue of a rabbit. Recently, silk fibroin functionalized with glycidyl-methacrylate (GMA) has been 3D printed by the digital lighting processing (DLP) technique and has been used for tissue regeneration (Fig. 10A).[88] The customized 3D-printed trachea demonstrated excellent chondrogenic differentiation with suitable biomechanical properties of the native rabbit trachea. The transplanted chondrocyte-laden silk-GMA hydrogel integrated into the surrounding structure by increasing the internal diameter after 6 weeks. Although the silk fibroin has been used in 3D

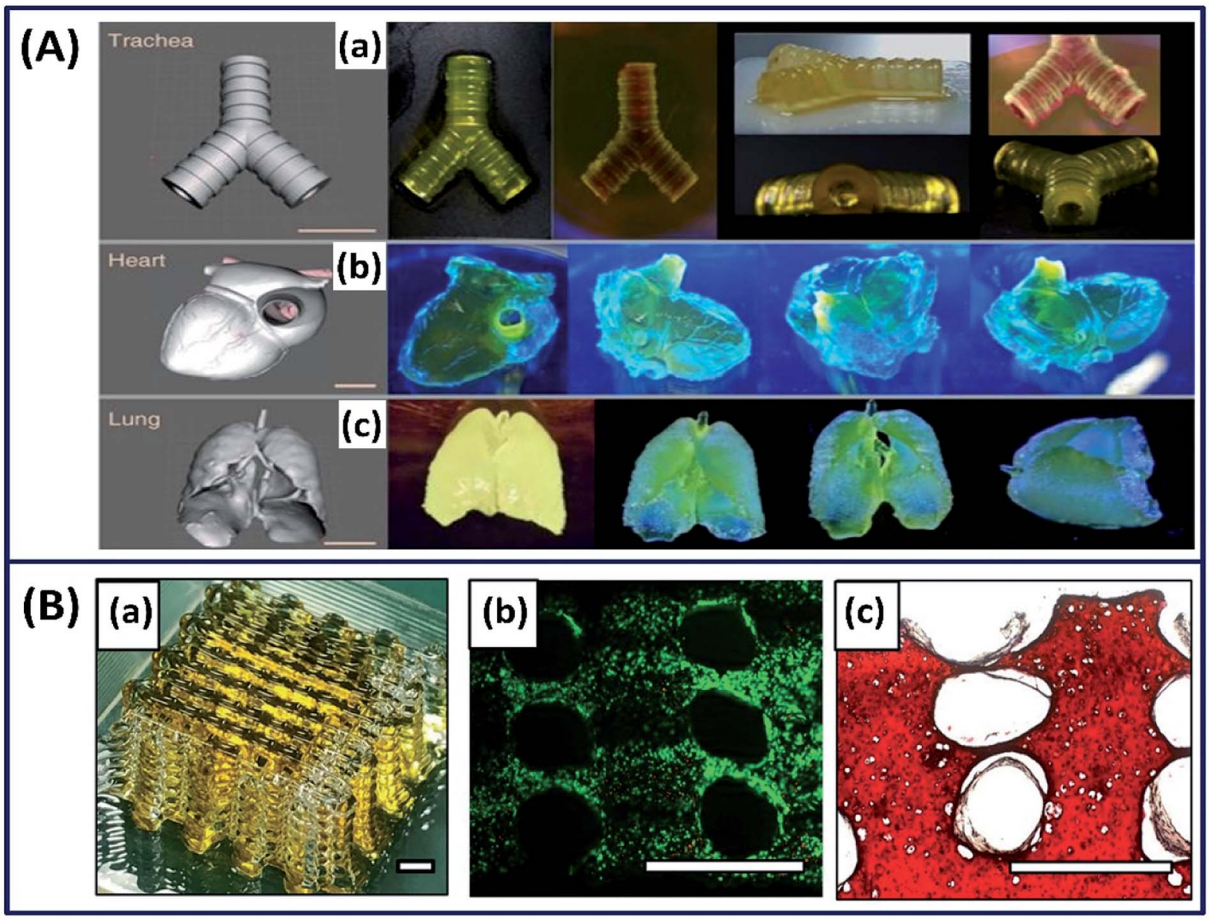

Fig. 9 (A) Images of CAD and 3D-printed complex structures using silk-MA. (a) Trachea, (b) heart and (c) lungs. Scale bar indicates 1 cm. Reprinted with permission from ref. 73 Copyright © 2018 Nature. (B) (a) Macroscopic image of the silk fibroin hydrogel by 3D printing process. (b) Live/dead images at day 1 (green-live, red-dead). (c) Safranin-O staining (red) at week 5. Scale bar = 1 mm. Reprinted with permission from ref. 26 Copyright © 2020 Wiley.

Open Access Article. Published on 08 September 2020. Downloaded on 1/22/2026 4:27:21 AM.
This article is licensed under a Creative Commons Attribution-NonCommercial 3.0 Unported Licence.

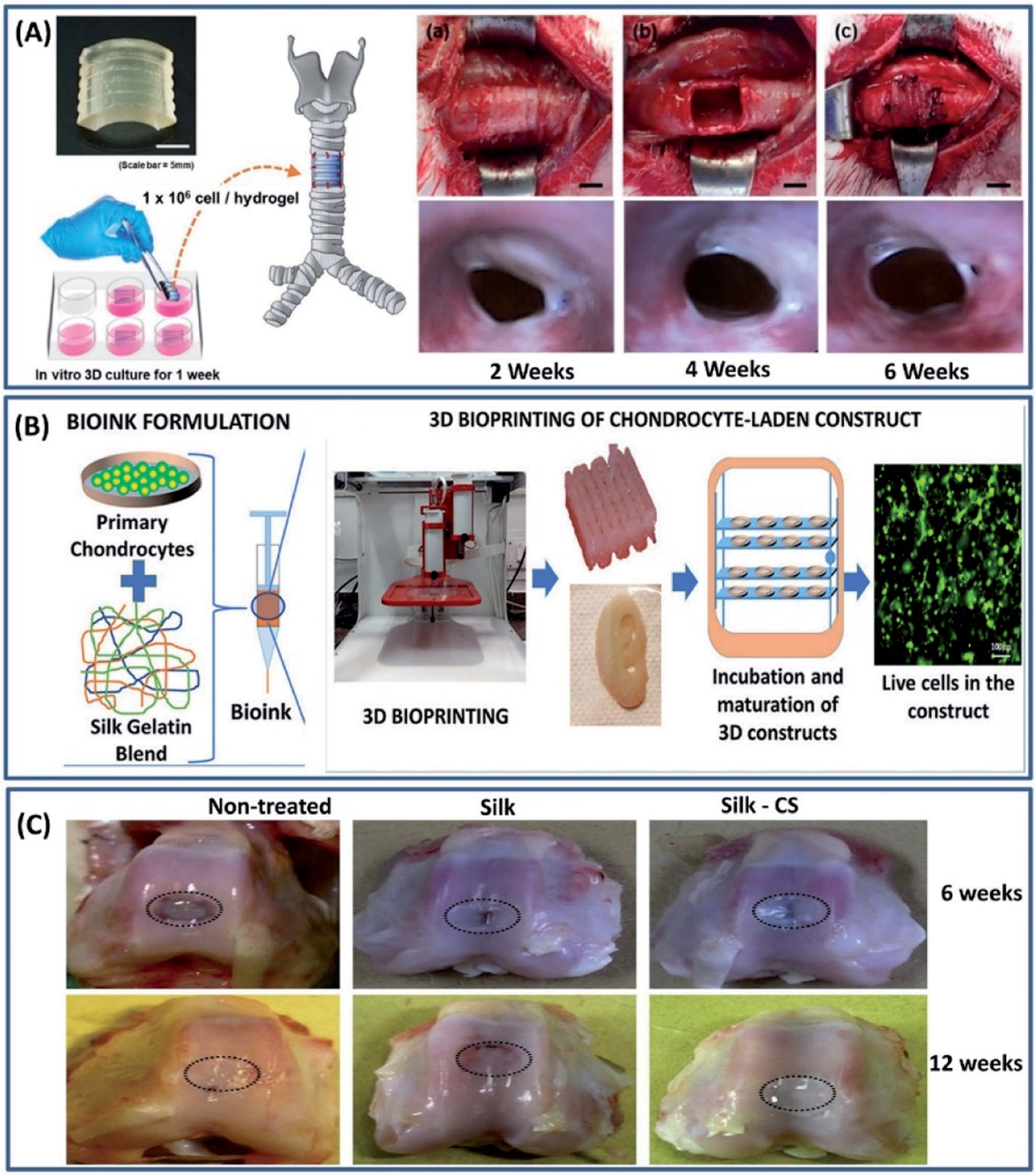

Fig. 10 (A) Artificial trachea printed by a DLP printer with chondrocytes from the rabbit ear and cultured for 1 week. (a and b) After cutting and removing the part of trachea, (c) artificial trachea was implanted. Scale bars represent 5 mm; endoscopy at 2, 4, and 6 weeks after trachea transplantation. Reproduced with permission from ref. 88 Copyright © 2020 Elsevier. (B) Scheme of the study showing bioink formulation and 3D bioprinting and maturation of cell-laden construct. Reprinted with permission from ref. 89 Copyright © 2019 American Chemical Society. (C) Macrophotographs showing the defects in the three experimental groups at 6 weeks (upper panels) and 12 weeks (lower panels) post surgery. Reproduced with permission from ref. 90 Copyright © 2017 Elsevier.

printing by employing different crosslinking mechanisms, the majority of the studies were employed post cell culture studies due to the cytotoxicity induced by the crosslinking agents. To overcome this, recently, Singh *et al.* have developed a cross-linker-free bio ink using silk fibroins, gelatin and chondrocyte cells to print cartilage tissues.[89] The biocompatible gelatin is

 This journal is © The Royal Society of Chemistry 2020

Open Access Article. Published on 08 September 2020. Downloaded on 1/22/2026 4:27:21 AM.
This article is licensed under a Creative Commons Attribution-NonCommercial 3.0 Unported Licence.

used to tune the rheological properties, thereby improving the overall printability. The 3D-printed cell-laden hydrogel exhibited a suitable microstructure, gelation, degradability and mechanical properties for the chondrogenic differentiation, demonstrating its suitability for cartilage tissue engineering (Fig. 10B). Silk fibroin constructs exhibit excellent mechanical strength and chondrogenic differentiation for cartilage repair but lack the anti-inflammation property. Therefore, silk fibroin has been combined with the chondroitin sulfate (CS) to improve the anti-inflammation property.[90] The genipin crosslinked 3D silk/CS hydrogel demonstrated superior mechanical property with increased cartilage formation and anti-inflammatory activities when compared to the native silk scaffold (Fig. 10C).

3.1.2 Bone tissue engineering

Bone tissue is one of the robust and complex tissue constructs of a human body, which comprises both organic (35%) and inorganic (65%) contents. The organic portion mainly consists of collagen, hyaluronan and proteoglycans, whereas the inorganic part consists of hydroxyapatite (HA) and salts.[31] The interesting properties of silk fibroins such as easy processability and tunable structural, mechanical and degradation properties along with the ability to support the stem cells to differentiate along the osteogenic lineage make them an attractive material for bone tissue repair.[91] The silk fibroin membrane made by lyophilization exhibits suitable mechanical properties and osteogenic differentiation, demonstrating its potential for bone formation.[92] Moreover, the mechanical and degradation characteristics can be tuned by ethanol treatment and the *in vivo* studies of these tuned silk films revealed that they are comparable to commercially available osteoguide and porcine collagen membranes, as shown in Fig. 11A. In other study, the silk fibroin films made by electrospinning demonstrated excellent adhesion, spreading and proliferation of human bone marrow stromal cells (BMSCs).[93] However, the fabricated structure cannot mimic the exact bone composition due to the absence of inorganic or mineral contents. To mimic the bone composition, hydroxyapatite (HA) is incorporated into the silk fibroin scaffold.[94] It is observed that there is an increase in mechanical strength (with time) and osteogenic differentiation of stem cells with an increase in HA content (Fig. 11C).[95] Moreover, the bone sialoprotein immunohistochemistry staining revealed an increase in bone matrix deposition over 10 weeks (Fig. 11D). In another study, the mineralization of the silk

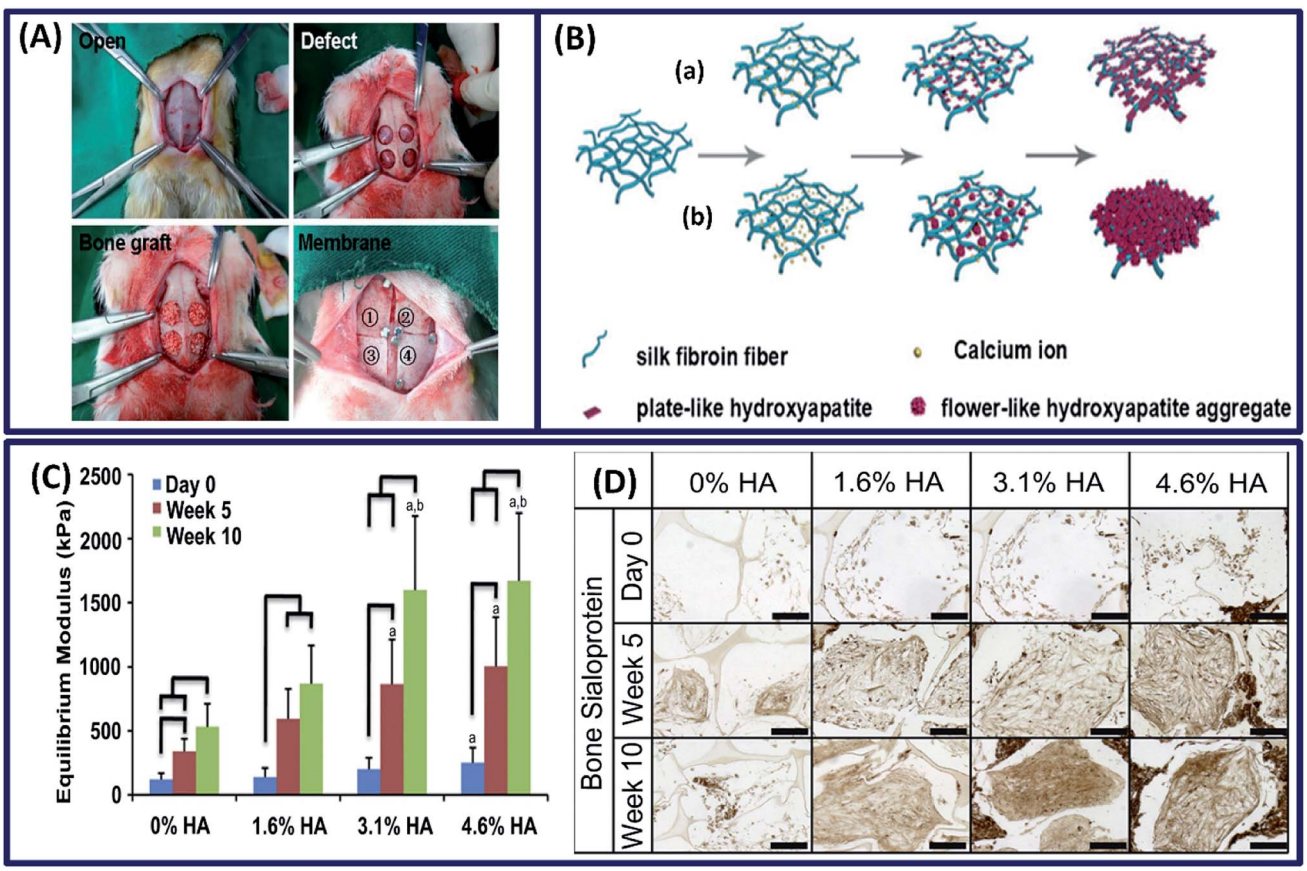

Fig. 11 (A) The whole surgical procedure. The experimental membrane was covered on the defects as follows: [1] silk1, [2] silk2, [3] Osteoguide and [4] porcine collagen. Reprinted with permission from ref. 92 Copyright © 2017 Elsevier. (B) Illustration of the formation of fibroin-directed hydroxyapatite with different Ca ion concentrations: (a) low concentration of calcium ions and (b) high concentration of calcium ions. Reprinted with permission from ref. 96 Copyright © 2015 Elsevier. (C) Equilibrium Young's modulus and (D) bone sialoprotein (scale: 200 μm) of the constructs after 5 and 10 weeks of cultivation. Reprinted with permission from ref. 95 Copyright © 2011 Elsevier.

Open Access Article. Published on 08 September 2020. Downloaded on 1/22/2026 4:27:21 AM.
This article is licensed under a Creative Commons Attribution-NonCommercial 3.0 Unported Licence.

hydrogel was done by a biomimetic method.[96] The silk scaffolds were made by a self-assembly mechanism and the *in vitro* mineralization was done using Na_2HPO_4 and calcium ions. The *in vitro* mineralization improved the compressive modulus and osteogenic activity of silk fibroin hydrogel, and the degree/rate of mineralization can be tuned by regulating the calcium ions (Fig. 11B). The resulting organic–inorganic scaffold mimics the bone composition and promotes the viability, proliferation and differentiation of osteoblasts, demonstrating its suitability for bone tissue engineering applications.

3.1.3 Neural tissue engineering

The nervous system is an essential and complex system in human architecture, which consists of mainly two components, namely, central nervous system (CNS) and peripheral nervous system (PNs). The malfunction of these neural systems due to disease or injury can cause fatal repercussions and curing them is extremely difficult due to its complex physiology and inadequate regenerative capacity.[97] The material design for neural tissue engineering should possess characteristics such as flexibility and moderate stiffness and can mimic the microenvironment to support cell distribution and promote axonal growth.[98] Among several natural polymers, silk fibroin is an excellent biomaterial that has the potential to demonstrate neural extension and axonal fasciculation with tunable stiffness (by altering the silk fibroin concentration).[99] To exploit the several advantageous properties of silk fibroin, it has been proposed for the repair of peripheral nerve tissues, where it demonstrated excellent biocompatibility with the peripheral nerve tissue and supported the growth of dorsal root ganglia (DRG) and facilitated the Schwann cell survival.[100] It is known that the neural tissue is electro-responsive and the electric signals can guide the differentiation of neural stem cells.[101] However, the silk fibroin is not a conductive material to induce the electric signals to guide neural differentiation. To overcome this problem, Dana *et al.* incorporated the gold nanoparticles into a silk fibroin matrix to improve the electrical conductivity and cellular response.[102] The resulting nanocomposite demonstrated excellent electrical conductivity, cellular attachment and neurogenic differentiation of PC12 cells. The *in vivo* studies on using silk fibroin/gold nanocomposites for peripheral nerve regeneration exhibited improved gait, standing, stretching and jumping of rats even after 10 months (Fig. 12A).[23] Moreover, the animals implanted with silk fibroin/gold nanoparticles and cells demonstrated nerve growth along the nerve gap and became completely normal after 18 months. The topography of the scaffold can also dictate the neurogenic differentiation by providing the topological cues to direct the axonal and neurite growth. For example, Nune *et al.* fabricated aligned and random

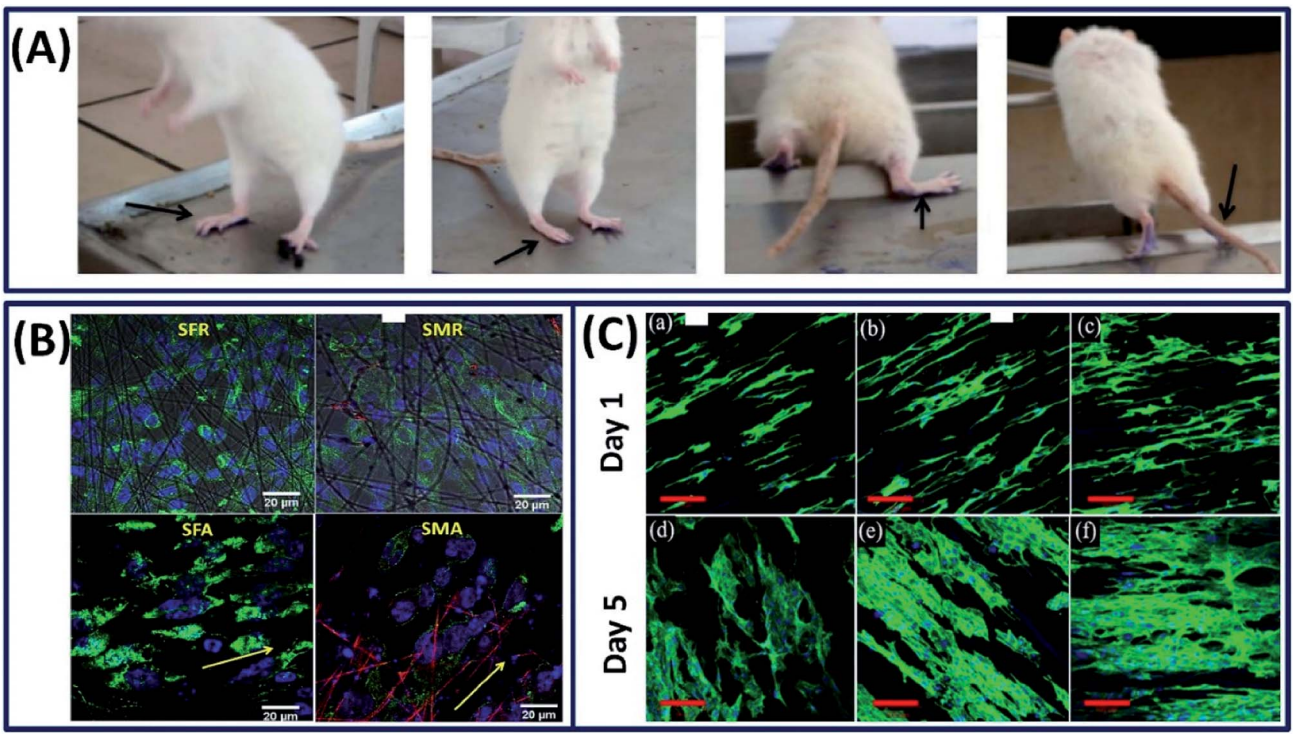

Fig. 12 (A) Animals implanted with silk/gold nano particle cell conduits exhibited improved gait and could stand, stretch and jump by the end of 10 months. Black arrows indicate the operated leg. Reprinted with permission from ref. 23 Copyright © 2015 Elsevier. (B) Cell differentiation using beta-tubulin staining for the neuroblastoma cells on the surface of the silk and silk/melanin random and aligned nanofibers after 3 days of culture confirming that they can favor and promote neuronal differentiation. Reprinted with permission from ref. 103 Copyright © 2019 Elsevier (C) confocal fluorescence micrographs of PC12 cells cultured on aligned nanofibers (a and d) pristine PU, (b and e) PU/silk fibroin, and (c and f) PU/silk-fMWCNTs respectively. Nuclei and actin filaments were stained with DAPI (blue) and actin-green respectively in fluorescence images. Reproduced with permission from ref. 104 Copyright © 2019 Elsevier.

 This journal is © The Royal Society of Chemistry 2020

Open Access Article. Published on 08 September 2020. Downloaded on 1/22/2026 4:27:21 AM.
This article is licensed under a Creative Commons Attribution-NonCommercial 3.0 Unported Licence.

electro-spun silk fibroin/melanin nanofibers for nerve tissue repair by electrospinning.[103] It is observed that the melanin-incorporated aligned silk nanofibers demonstrated a well-extended oriented morphology and high neuronal differentiation marker expression when compared to the random silk nanofibers (Fig. 12B). Similarly, aligned scaffolds of polyurethane (PU) combined with the silk fibroin functionalized with the multi-walled carbon nanotubes demonstrated excellent neuro-regeneration when compared with the random topography. The presence of multi-walled carbon nanotubes (MWCNTs) significantly improved the electrical conductivity of the scaffold, thereby enhancing the proliferation of Schwann cells and differentiation of PC12 cells by guiding them along the axis of fiber alignment.[104] From the fluorescence images, it is clearly observed that the aligned PU/silk-MWCNT conductive nanofibrous scaffold provides an excellent bio-interface that can support the axonal regeneration for the fast healing of peripheral nerves (PNs) (Fig. 12C). Apart from making the aligned silk fiber scaffolds, incorporating growth factors into aligned fibers is also a general strategy to improve the neurite growth. By employing this approach, Wittmer *et al.* increased (2–3 times) the growth of neurites by adding brain-derived neurotrophic factor (BDNF) and ciliary neurotrophic factor (CNTF) without altering the structure and surface morphology of the electrospun aligned silk fibers.[105] The increase in neurite activity promoted nerve growth and axon regeneration in the central nervous system, demonstrating its potential as a biomaterial for neuro-regenerative applications.

Overall, the versatility of silk fibroin fabrication/processing into multiscale dimension with structural (nano–micro) tunability and the capability of incorporating biological cues and conducting polymers into a 3D matrix made it a suitable candidate for a wide range of tissue constructs with increased biological performance.

3.2 Bioelectronics

Bioelectronics is an emerging branch in the current healthcare system because of its excellent features such as personalized health care, early disease diagnosis and minimally invasive treatment.[106] The development of bioelectronic devices requires expertise from various fields including biomedical scientists, electronic engineers and materials scientists, as such devices should possess essential characteristics such as biocompatibility, degradability (tunable), conductivity, stability and flexibility to integrate into curvilinear biological tissue constructs.[107] Among various natural proteins, the silk fibroin is a sustainable protein that possesses all the tunable structural, mechanical and degradation properties along with the ability to incorporate conductive materials and conducting polymers.[108] Besides, silk fibroins can be made electrically conductive by converting them

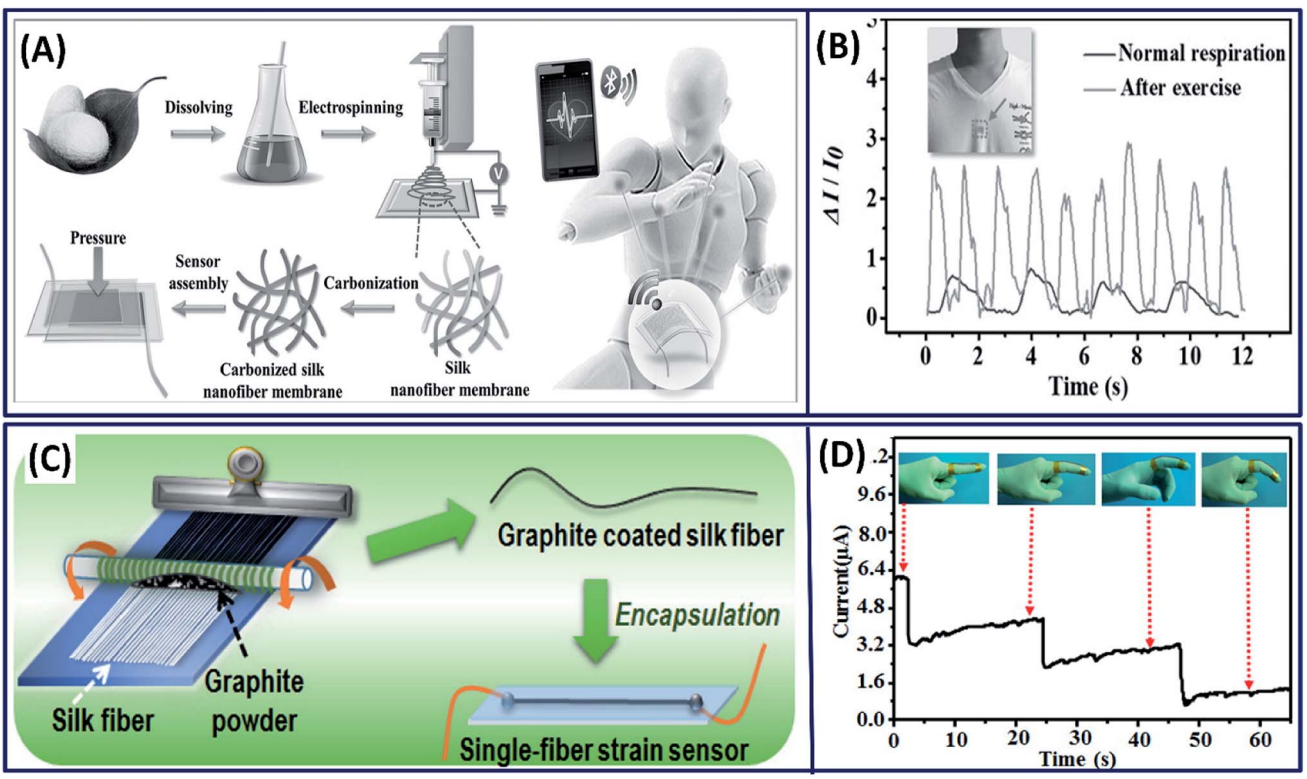

Fig. 13 (A) Schematic showing the fabrication process of carbonized silk nano-membrane (CSilkNM) pressure sensors. Real-time and *in situ* human physiology monitoring and the prosthetic touch simulation. (B) Respiration wave monitoring under normal and exercise conditions. Reproduced with permission from ref. 24 Copyright © 2017 Wiley. (C) Schematic showing the fabrication process. (D) Response of the wearable sensor to stepwise bending of an index finger (insets show photographs of a strain sensor attached along a finger, using an adhesive tape). Reproduced with permission from ref. 112 Copyright © 2016 American Chemical Society.

Open Access Article. Published on 08 September 2020. Downloaded on 1/22/2026 4:27:21 AM.
This article is licensed under a Creative Commons Attribution-NonCommercial 3.0 Unported Licence.

into sp^2-hybridized N-doped carbon materials by pyrolysis because of their molecular structure and nitrogen content.[109] The silk fibroin obtained after pyrolysis is termed silk-derived carbon materials, which is highly conductive and can be explored in various soft electronic applications such as wearable electronics and implantable devices.

3.2.1 Wearable bioelectronic sensors. Wearable electronic devices on the human skin that can monitor the health and well-being are continuously attracting significant attention in the current medical treatment because of their ability to detect the diseases at early stages.[110] To detect the abnormal/disease signals using these wearable devices, they must be capable of detecting the highly sensitive physiological signals.[111] It is known that the carbonized silk fibroin is highly conductive and capable of detecting low signals with high sensitivity. Based on this, Wang *et al.* developed a transparent and highly sensitive electronic skin by carbonizing the electrospun silk fibroin fibers to detect the pressure changes in the body (Fig. 13A).[24] The pressure changes are obtained by correlating with the observed current differences when exposed to physiological stimuli. The performance of the pressure sensors can be tuned by varying the thickness of the silk fibers, demonstrating the highest sensitivity (34.47 kPa^{-1}) of the fibers with lower thickness and fast response (<16.7 ms) with low detectable pressure (0.8 Pa). The electronic skin is capable of detecting the wrist pulse and respiration before and after exercise (Fig. 13B). The amalgamation of conductive materials with silk fibers is another strategy to fabricate flexible electronics. Adapting this approach, Zhang *et al.* fabricated a low cost and highly sensitive motion detectable wearable strain sensor by simply coating the electrically conductive graphite onto silk fibers by a dry-Meyer-rod-coating process (Fig. 13C).[112] The fabricated single fiber strain sensor demonstrated high sensitivity with a wide workable strain range of 0–15% with high resilience (>3000 cycles) and can be utilized as a motion detection sensor (Fig. 13D). In other study, the water-soluble graphene oxide is coated onto the silk fibers initially and reduced chemically to form electrically conductive silk/graphene fiber films.[113] The fabricated films are highly flexible, mechanically strong with excellent electrical conductivity and could be used as a potential candidates for the diagnosis of diabetes because of their excellent glucose-sensing capability.

The sensitive interactions between water molecules and silk fibroin chains is a valuable property that can be exploited for the development of humidity sensors. Based on the absorption and desorption of water molecules with silk fibroin molecular chains, a highly efficient and sensitive humidity sensor is made by blade coating of silk fibroins on a silver/polyethylene

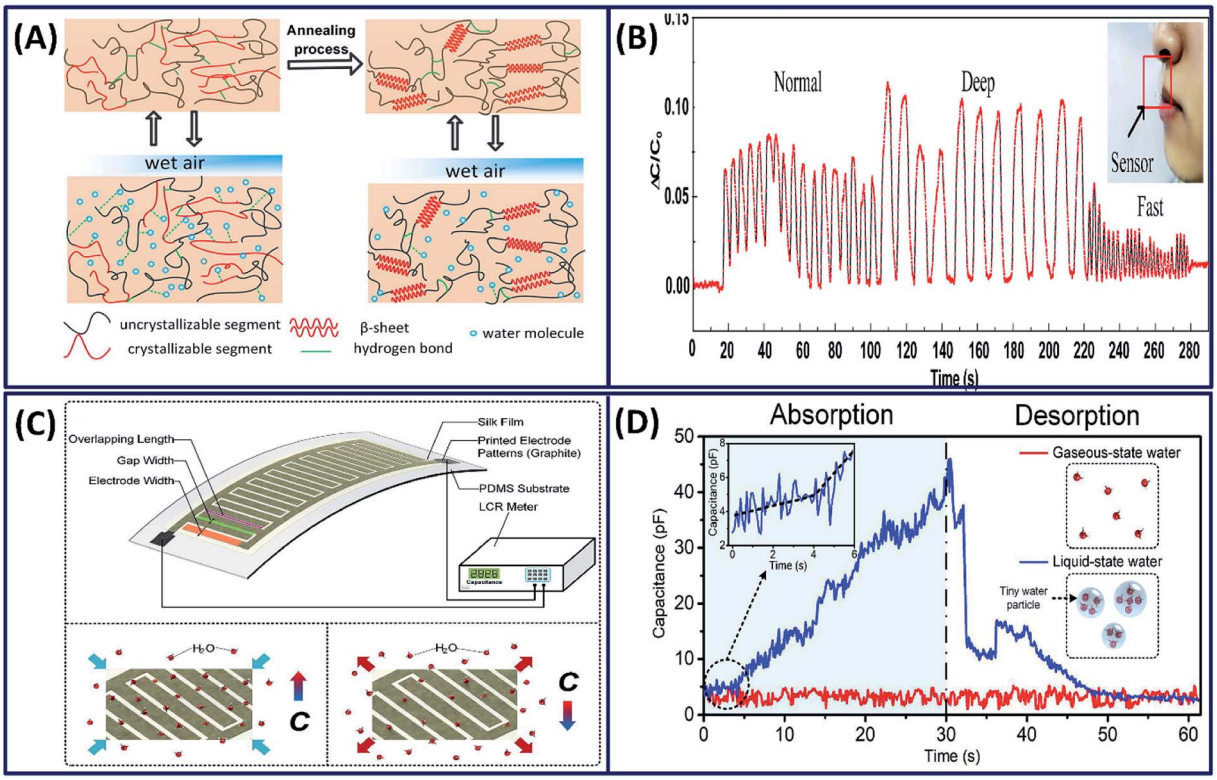

Fig. 14 (A) Illustration of principles for water molecule absorption and desorption inside intrinsic and modified SF molecule chains. (B) Capacitance response of the sensor for different breathing rates and intensities. Reprinted with permission from ref. 114 Copyright © 2020 Elsevier. (C) Working principle and measurement platform of the proposed wearable silk electronic device and the mechanism of absorption and desorption of water molecules, resulting in an increase and a decrease in capacitance respectively. (D) The absorption–desorption spectra of the electronic device when exposed to liquid- and gaseous-state water molecules. Reprinted with permission from ref. 115 Copyright © 2019 Elsevier.

 This journal is © The Royal Society of Chemistry 2020

Open Access Article. Published on 08 September 2020. Downloaded on 1/22/2026 4:27:21 AM.
This article is licensed under a Creative Commons Attribution-NonCommercial 3.0 Unported Licence.

terephthalate (Ag/PET) substrate (Fig. 14A).[114] The escaping difference between bound and unbound moisture during breathing alters the dielectric constant of the sensing film and influences the capacitance of the sensor. It is observed that the capacitance response clearly distinguishes the different types of breathing such as normal, deep and fast (Fig. 14B). Similarly, the silk fibroin is coated onto the PDMS/graphite electrode film to fabricate a flexible humidity sensor, which has the capability to distinguish the liquid- and gaseous-state water molecules (Fig. 14C).[115] The capacitance of the film is constant when exposed to gaseous water molecules, whereas the absorption of liquid water molecules increased the capacitance, clearly detecting the different states of water (Fig. 14D). In addition to the humidity sensor, it has multifunctional capabilities in detecting the breath variations and human joint movements.

3.2.2 Implantable electronic devices. The implantable electronic devices are the biocompatible devices containing electronic components, which have attracted significant attention in modern biomedicine.[116] These implantable devices are capable of detecting the diseases and curing them *in vivo* wirelessly.[117] Often, these devices contain non-degradable electronic components that can cause the inflammatory response sometimes. However, a good balance between the electronic components and the bulk material for device fabrication can minimize the toxic biological response. For instance, the electronic nano-membrane silicon integrated into the thin silk fibroin (bulk material) flexible film demonstrated excellent dissolution *in vivo* and no inflammation around the implant site in mice (Fig. 15A).[21] The fabricated electronic device is mechanically flexible with excellent electron mobility,

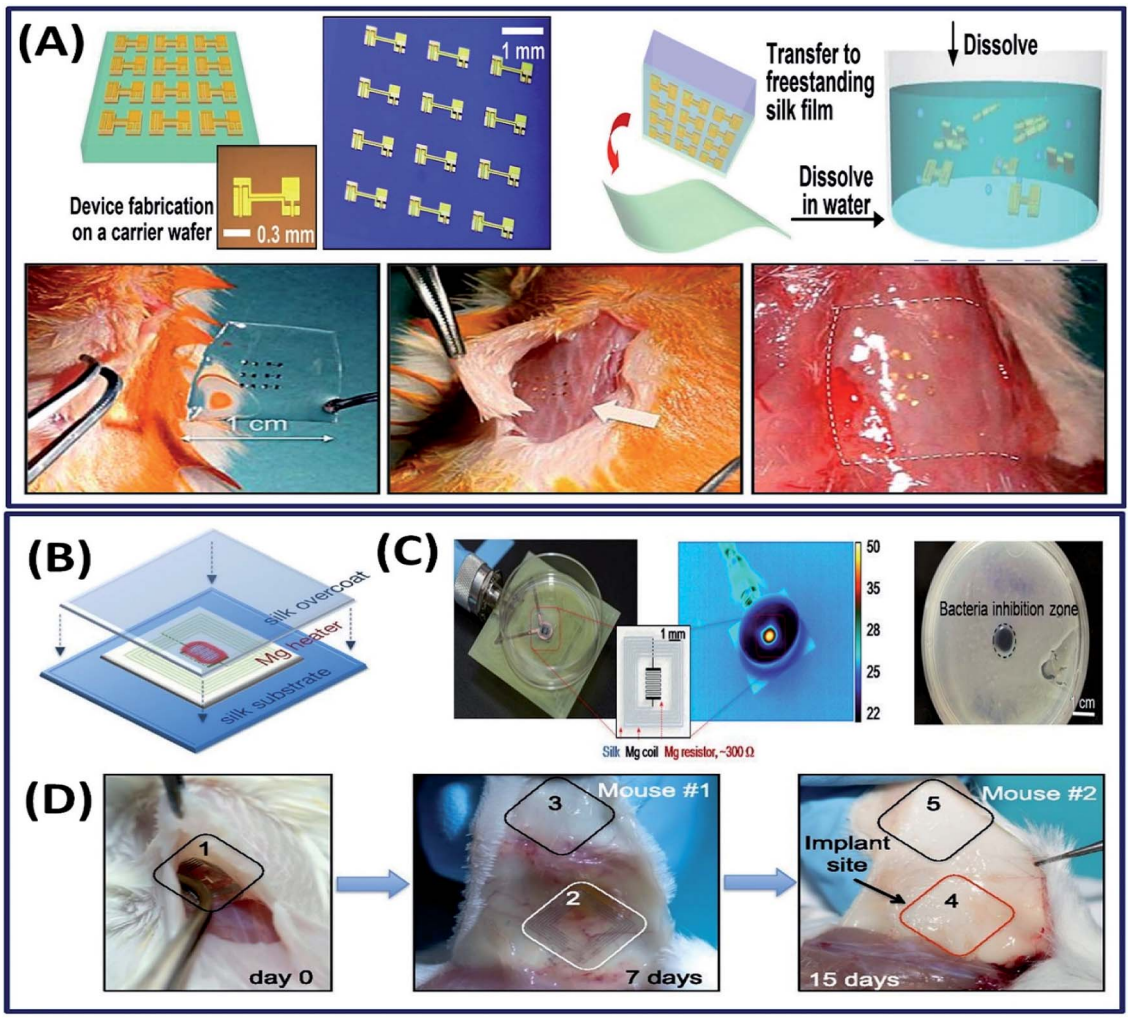

Fig. 15 (A) Schematic of ultrathin devices on a carrier wafer, transfer printing onto a freestanding silk film followed by dissolution and the procedure of the animal toxicity test: image before (left) and shortly after (center) and two weeks after (right) implantation. Reprinted with permission from ref. 21 Copyright © 2009 AIP Publishing. (B) The Mg heater was encapsulated in a silk "pocket" that protects the electronics and can be used to program the lifetime of the device. *In vitro*: (C) the devices were placed underneath bacterial cultures of *S. aureus* grown on agar plates and powered to achieve a desired temperature, monitored using an IR camera. A clear zone of inhibition, after heat treatment and overnight incubation, appeared in correspondence to the area of heat treatment application. (D) Monitoring of device degradation and tracing of Mg ions. Devices were implanted and examined after 7 and 15 days. Reprinted with permission from ref. 119 Copyright © 2014 National Academy of Sciences USA.

Open Access Article. Published on 08 September 2020. Downloaded on 1/22/2026 4:27:21 AM.
This article is licensed under a Creative Commons Attribution-NonCommercial 3.0 Unported Licence.

demonstrating its suitability as a bioresorbable electronic implant. In general, the implanted electronic devices often need to be removed after the desired functional outcome is achieved; requiring post-surgical procedures, which sometimes disrupt the cured tissue.[118] To overcome this, Tao *et al.* fabricated a thermal therapeutic device that can be controlled wirelessly after implantation.[119] Briefly, Mg and MgO are deposited onto silk fibroin substrates, which act as resistors and power-receiving coils and wirelessly powered by near field inductive coupling (Fig. 15B). The fabricated device is used to enhance bacterial inhibition by wirelessly controlling the temperature (Fig. 15C). The *in vivo* studies revealed that the implanted device is degraded completely after 15 days with no material residues (Fig. 15D). In another study, gold nanoparticle-doped silk fibroin films with other thermo-electronic components were used to power the implanted electronic devices wirelessly.[120] As a proof of concept, the study established that the electronic device can generate electricity wirelessly by heating the thermo electronic element, triggered by external light. However, the practical application and *in vivo* studies need to be established to demonstrate its suitability for translational research. Although preliminary investigation on the use of silk fibroin constructs as implantable electronic devices demonstrated satisfactory results, the number of studies on the utilization of silk fibroins in implantable electronics is very limited. There is significant scope in capitalizing the excellent tunable characteristics of silk fibroins in the implantable electronic device industry.

3.3 Drug delivery

The ability to process/fabricate the silk fibroin into multiscale dimensions like nano–micro-particles, thin films and hydrogels made it an ideal candidate for the delivery of drugs and genes. In general, the silk drug delivery devices are made by directly dissolving or incorporating the drug molecules into a silk fibroin solution followed by fabrication into different morphologies.[30] The molecular weight of a drug and its physiochemical interactions with the silk construct play an important role in determining the drug release kinetics. For example, the release rate of dextran incorporated into silk films is inversely proportional to the dextran molecular weight.[121] Oral drug delivery (discussed in Section 2.1) is a globalized way, and

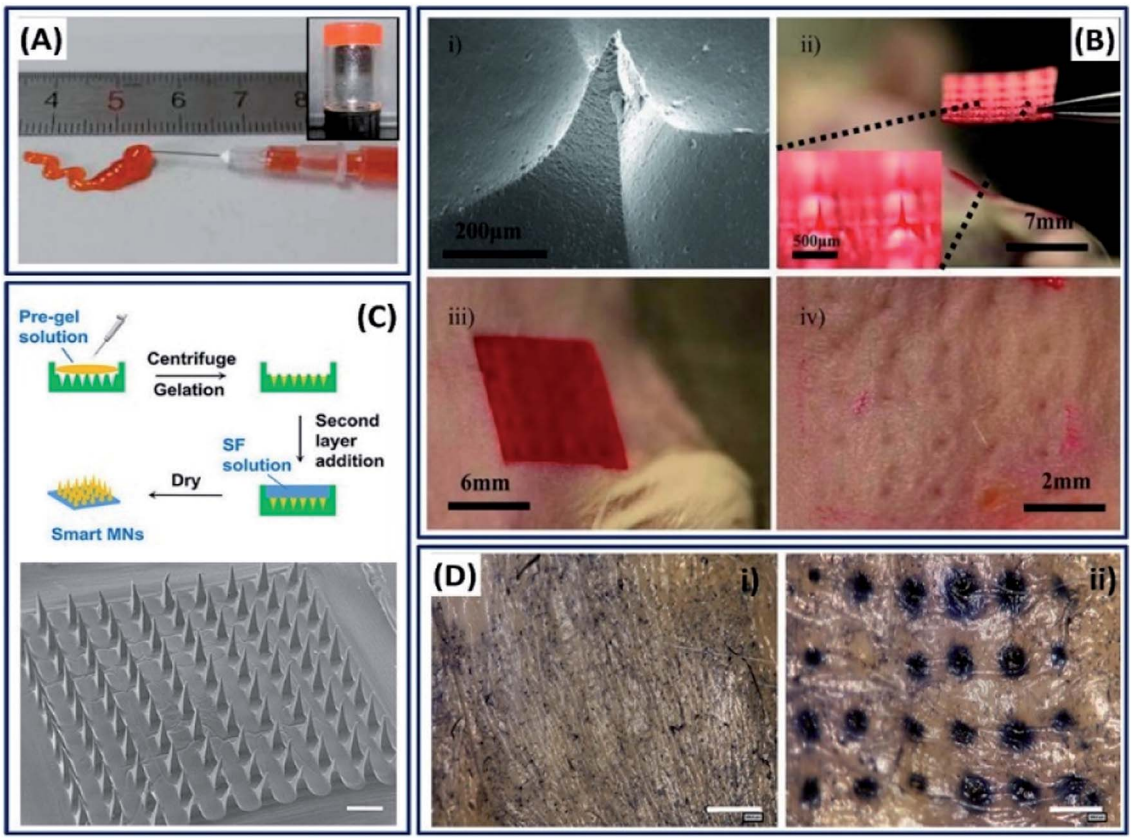

Fig. 16 (A) Injectability of silk fibroins from a prefilled syringe and inverted vial image. Reprinted with permission from ref. 124 Copyright © 2016 American Chemical Society. (B) Silk microneedles as applied to mouse skin: (i) SEM image of an individual silk microneedle, (ii) silk microneedle patch, relative size comparison to mouse, (iii) silk microneedle patch applied to animal skin, (iv) skin after removal of microneedle patch; needle penetration marks are clearly visible. Reprinted with permission from ref. 22 Copyright © 2011 Wiley. (C) Schematic and morphology of the micro-needle fabricated with SF-combined semi-IPN hydrogel as a needle tip and SF as a base layer. Scale bar: 500 μm. (D) *In vitro* skin insertion capability. Mouse skin was treated (i) without or (ii) with smart hybrid micro-needles for 10 min and stained with trypan blue to indicate the formation of microchannels. Reprinted with permission from ref. 126 Copyright © 2019 American Chemical Society.

Open Access Article. Published on 08 September 2020. Downloaded on 1/22/2026 4:27:21 AM.
This article is licensed under a Creative Commons Attribution-NonCommercial 3.0 Unported Licence.

in some cases, it is not so effective. Localized drug delivery is critical in some cases such as tumors, because of maintaining high drug concentrations at the site by avoiding drug loss during transportation.[122] Injectable hydrogels are promising candidates for the localized drug delivery, in which the drug-loaded solution is transformed into a gel by either physical or chemical crosslinking under physiological conditions for controlled release kinetics.[123] For example, a pH-responsive thixotropic injectable silk fibroin hydrogel is used for the localized delivery of doxorubicin (DOX) for breast cancer therapy.[124] Due to the thixotropic property, the drug-loaded silk fibroin solution is transformed into the solid after immediate injection (Fig. 16A). The injection of drug-loaded silk hydrogel into the breast cancer model showed anticancer capacity, demonstrating the suitability of injectable silk hydrogels for localized chemotherapy. Apart from conventional drug-encapsulated crystals and injectable hydrogels, microneedles are drawing considerable attention and emerging as more efficient and minimally invasive drug delivery devices.[125] For instance, Tsioris *et al.* developed a drug-loaded silk microneedle at ambient temperature and pressure by simply casting the silk fibroin solution into a PDMS mold created by an aluminum microneedle master.[22] The fabricated silk microneedle patch successfully penetrated the underlying tissue of a mouse, demonstrating its mechanical strength (Fig. 16B). The drug release kinetics in microneedles can also be tuned by controlling the protein secondary structure by altering the post-processing conditions. The ambient fabrication conditions favored the bulk loading of biological and temperature-sensitive drugs such as antibiotics, peptides and vaccines. Recently, silk fibroin microneedles have been used for glucose-responsive insulin delivery.[126] The microneedles are made of semi-interpenetrating networks of silk fibroin and phenylboronic acid/acrylamide. Instead of general single-step microneedle fabrication, a two-layer strategy is employed to improve the sensitivity with the glucose in which the base layer is made of

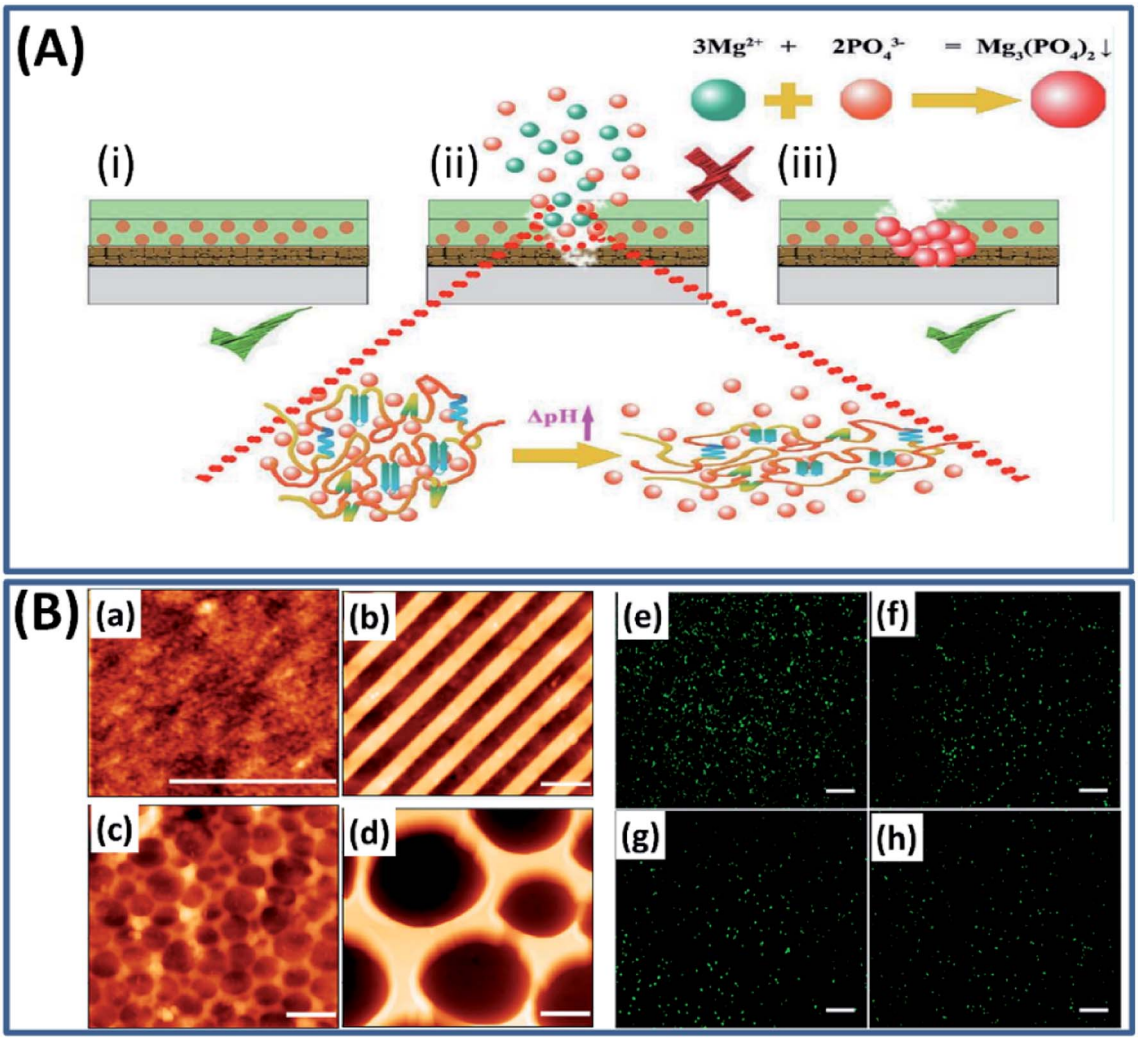

Fig. 17 (A) Schematic of the self-healing mechanism upon silk–KP exposure in the immersion environment. Reproduced with permission from ref. 25 Copyright © 2019 Elsevier. (B) AFM topography images (a–d) (scale bars, 2 μm) and fluorescent microscopy images (e–h) (scale bars, 50 μm) of GFP expressing bacteria cultured after 24 hours on flat silk (a and e), nano stripes (b and f), μ wells 1 (c and g), and μ wells 2 (d and h) samples. Reproduced with permission from ref. 133 Copyright © 2020 American Chemical Society.

Open Access Article. Published on 08 September 2020. Downloaded on 1/22/2026 4:27:21 AM.
This article is licensed under a Creative Commons Attribution-NonCommercial 3.0 Unported Licence.

silk fibroins and the needle region is made of silk fibroins and phenylboronic acid/acrylamide interpenetrating networks (Fig. 16C). The drug-loaded microneedles are mechanically robust and forming microchannels on the mouse skin, indicating that the needles penetrated into the stratum corneum for the delivery of insulin painlessly and safely (Fig. 16D).

3.4 Biocompatible coatings

Apart from the use of silk fibroin constructs as drug carriers, tissue scaffolds and bio-electronic devices, they have been used as coatings to tune the kinetics of a drug delivery process and degradation time and to improve the biocompatibility of the implants.[127,128] For example, the nanoscale silk fibroin film coated on different substrates by single-layer adsorption demonstrated excellent adhesion, growth and differentiation of human bone marrow stem cells.[129] The nanoscale film formed by the self-assembly mechanism can control or tune the interfacial properties of the biomedical implants.[130] Silk fibroin has been coated on a titanium bone implant by electro-deposition and functionalized with bioactive compounds to tune the regenerative tissue microstructure.[131] The implants such as magnesium alloys possess excellent mechanical and biological properties, yet their utility as implants is often restricted by their corrosive nature, inability to self-repair and fast degradation rates.[132] To overcome this problem, a pH-sensitive self-healing coating is made from silk fibroin and K_3PO_4 to improve the corrosion resistance and self-healing capability of the magnesium implant.[25] Briefly, when the implant is corroded, Mg^{2+} ions are released, which increase the local pH. At the same time, the change in pH triggers silk fibroin conformational changes and releases PO_4^{3-} ions present in the silk–KP complex. The Mg^{2+} and PO_4^{3-} ions react immediately to form a $(Mg)_3(PO_4)_2$ complex, which immediately heals the corroded surface (Fig. 17A). The silk fibroin acted as a skeleton coating and improved the osteogenic activity, whereas PO_4^{3-} ions (the inorganic ingredient of bone) act as a corrosion inhibitor. Very recently, the silk fibroin construct has been used as an antifouling substrate with different nano and microstructure topographies using a soft lithographic approach to prevent bacterial colonization.[133] This study revealed important facts such as the surface topography has a significant influence on the antifouling capacity by demonstrating the reduction in bacterial adhesion by 66% on structured surfaces when compared to an unpattern surface (Fig. 17B).

4 Conclusions and outlook

In summary, we discussed the fundamentals of processing silk fibroins in multiscale dimensions by both conventional approaches and using advanced methodologies to leverage their use in diverse biomedical applications. The silk particles are mostly utilized as drug carriers, and the size of particles are mainly controlled by adopting a suitable strategy and tuning the process variables. The film and hydrogel/scaffold forms of silk fibroins are mainly made by physical and chemical crosslinking mechanisms and they are widely explored in coatings and tissue engineering applications. The capacity of silk fibroin constructs to mimic the physiochemical characteristics of various natural tissue constructs and the ability to incorporate the biological cues for the desired cellular activities made them the most interesting materials for tissue engineering applications. Moreover, the ability to adapt 3D printing technologies by tuning its rheological characteristics made it possible to mimic the exact architecture of complex biological structures such as lungs, heart, and cartilage. In the past, the desired silk fibroin architecture or morphology is achieved by adopting appropriate processing methods and mechanisms. However, using the recent design-driven advanced technologies such as lithography and 3D printing, the architecture of silk fibroin constructs can be controlled across different length scales (nano–micro–macro). The utilization of these advanced technologies made it possible to fabricate silk fibroin constructs in defined micro- and nano-patterns by incorporating microelectronics, which opened a whole new window for the use of silk fibroin in wearable electronic sensors and implantable electronic devices. Overall, the simultaneous progress in understanding the fundamentals of tunable silk fibroin structures (in multiscale dimension) and advanced computer-aided manufacturing technologies opened different platforms for its exploration in biomedicine. The continuation of research on silk-based materials coupled with advanced fabrication technologies would certainly transform our contemporary biomedicine to sustainable green biomedicine in the near future.

Conflicts of interest

The authors declare no conflict of interest.

Acknowledgements

The authors acknowledge the School of Graduate Research (SGR), RMIT University for providing the PhD scholarship for one of the authors (PD). The research has been supported by Australian Research Council (ARC) funding through discovery project.

References

1 T. D. Sutherland, J. H. Young, S. Weisman, C. Y. Hayashi and D. J. Merritt, *Annu. Rev. Entomol.*, 2010, **55**, 171–188.
2 C. Fu, Z. Shao and V. J. C. C. Fritz, *Chem. Commun.*, 2009, 6515–6529.
3 Z. Zhu, Y. Kikuchi, K. Kojima, T. Tamura, N. Kuwabara, T. Nakamura and T. Asakura, *J. Biomater. Sci., Polym. Ed.*, 2010, **21**, 395–411.
4 A. Datta, A. K. Ghosh and S. C. Kundu, *Insect Biochem. Mol. Biol.*, 2001, **31**, 1013–1018.
5 R. Valluzzi, S. Winkler, D. Wilson and D. L. Kaplan, *Philos. Trans. R. Soc., B*, 2002, **357**, 165–167.
6 J. G. Hardy, L. M. Römer and T. R. Scheibel, *Polymer*, 2008, **49**, 4309–4327.
7 S. Inoue, K. Tanaka, F. Arisaka, S. Kimura, K. Ohtomo and S. Mizuno, *J. Biol. Chem.*, 2000, **275**, 40517–40528.

 This journal is © The Royal Society of Chemistry 2020

Open Access Article. Published on 08 September 2020. Downloaded on 1/22/2026 4:27:21 AM.
This article is licensed under a Creative Commons Attribution-NonCommercial 3.0 Unported Licence.

8 C. Z. Zhou, F. Confalonieri, M. Jacquet, R. Perasso, Z. G. Li and J. Janin, *Proteins: Struct., Funct., Bioinf.*, 2001, **44**, 119–122.
9 B. Lotz and F. Colonna Cesari, *Biochimie*, 1979, **61**, 205–214.
10 Z. Shao and F. Vollrath, *Nature*, 2002, **418**, 741.
11 C. L. Craig and C. Riekel, *Comp. Biochem. Physiol., Part B: Biochem. Mol. Biol.*, 2002, **133**, 493–507.
12 X. Li, J. Zhang, Y. Feng, S. Yan, Q. Zhang and R. You, *Polym. Degrad. Stab.*, 2018, **147**, 57–63.
13 D. Umuhoza, F. Yang, D. Long, Z. Hao, J. Dai and A. Zhao, *ACS Biomater. Sci. Eng.*, 2020, **6**, 1290–1310.
14 C. Holland, K. Numata, J. Rnjak-Kovacina and F. P. Seib, *Adv. Healthcare Mater.*, 2019, **8**, 1800465.
15 B. Kundu, N. E. Kurland, S. Bano, C. Patra, F. B. Engel, V. K. Yadavalli and S. C. Kundu, *Prog. Polym. Sci.*, 2014, **39**, 251–267.
16 J. Whittaker, R. Balu, N. R. Choudhury and N. K. Dutta, *Polym. Int.*, 2014, **63**, 1545–1557.
17 P. Shi and J. C. H. Goh, *Int. J. Pharm.*, 2011, **420**, 282–289.
18 N. Lin, G. W. Toh, Y. Feng, X. Y. Liu and H. Xu, *J. Mater. Chem. B*, 2014, **2**, 2136–2143.
19 M. C. Lee, D.-K. Kim, O. J. Lee, J.-H. Kim, H. W. Ju, J. M. Lee, B. M. Moon, H. J. Park, D. W. Kim, S. H. Kim and C. H. Park, *J. Biomed. Mater. Res., Part B*, 2016, **104**, 508–514.
20 D. Kuang, F. Jiang, F. Wu, K. Kaur, S. Ghosh, S. C. Kundu and S. Lu, *Int. J. Biol. Macromol.*, 2019, **134**, 838–845.
21 D.-H. Kim, Y.-S. Kim, J. Amsden, B. Panilaitis, D. L. Kaplan, F. G. Omenetto, M. R. Zakin and J. A. Rogers, *Appl. Phys. Lett.*, 2009, **95**, 133701.
22 K. Tsioris, W. K. Raja, E. M. Pritchard, B. Panilaitis, D. L. Kaplan and F. G. Omenetto, *Adv. Funct. Mater.*, 2012, **22**, 330–335.
23 S. Das, M. Sharma, D. Saharia, K. K. Sarma, M. G. Sarma, B. B. Borthakur and U. Bora, *Biomaterials*, 2015, **62**, 66–75.
24 Q. Wang, M. Jian, C. Wang and Y. Zhang, *Adv. Funct. Mater.*, 2017, **27**, 1605657.
25 P. Xiong, J. Yan, P. Wang, Z. Jia, W. Zhou, W. Yuan, Y. Li, Y. Liu, Y. Cheng, D. Chen and Y. Zheng, *Acta Biomater.*, 2019, **98**, 160–173.
26 X. Cui, B. G. Soliman, C. R. Alcala-Orozco, J. Li, M. A. M. Vis, M. Santos, S. G. Wise, R. Levato, J. Malda, T. B. F. Woodfield, J. Rnjak-Kovacina and K. S. Lim, *Adv. Healthcare Mater.*, 2020, **9**, 1901667.
27 A. Leal-Egaña, G. Lang, C. Mauerer, J. Wickinghoff, M. Weber, S. Geimer and T. Scheibel, *Adv. Eng. Mater.*, 2012, **14**, B67–B75.
28 A. Leal-Egaña and T. Scheibel, *J. Mater. Chem.*, 2012, **22**, 14330–14336.
29 M. K. DeBari, M. N. Keyser, M. A. Bai and R. D. Abbott, *Connect. Tissue Res.*, 2018, **61**, 163–173.
30 E. Wenk, H. P. Merkle and L. Meinel, *J. Controlled Release*, 2011, **150**, 128–141.
31 J. Melke, S. Midha, S. Ghosh, K. Ito and S. Hofmann, *Acta Biomater.*, 2016, **31**, 1–16.
32 T. P. Nguyen, Q. V. Nguyen, V.-H. Nguyen, T.-H. Le, V. Q. N. Huynh, D.-V. N. Vo, Q. T. Trinh, S. Y. Kim and Q. V. Le, *Polymers*, 2019, **11**, 1933.
33 Z. Xu, L. Shi, M. Yang and L. Zhu, *Mater. Sci. Eng. C*, 2019, **95**, 302–311.
34 F. Mottaghitalab, M. Farokhi, M. A. Shokrgozar, F. Atyabi and H. Hosseinkhani, *J. Controlled Release*, 2015, **206**, 161–176.
35 Z. Zhao, Y. Li and M. B. Xie, *Int. J. Mol. Sci.*, 2015, **16**, 4880–4903.
36 H.-J. Jin and D. L. Kaplan, *Nature*, 2003, **424**, 1057–1061.
37 W. Lohcharoenkal, L. Wang, Y. C. Chen and Y. Rojanasakul, *BioMed Res. Int.*, 2014, **2014**, 180549.
38 P. C. Bessa, E. R. Balmayor, H. S. Azevedo, S. Nürnberger, M. Casal, M. van Griensven, R. L. Reis and H. Redl, *J. Tissue Eng. Regener. Med.*, 2010, **4**, 349–355.
39 T. Imsombut, Y. Srisuwan, P. Srihanam and Y. Baimark, *Powder Technol.*, 2010, **203**, 603–608.
40 A. S. Lammel, X. Hu, S.-H. Park, D. L. Kaplan and T. R. Scheibel, *Biomaterials*, 2010, **31**, 4583–4591.
41 T. Tanaka, T. Tanigami and K. Yamaura, *Polym. Int.*, 1998, **45**, 175–184.
42 X. Wang, T. Yucel, Q. Lu, X. Hu and D. L. Kaplan, *Biomaterials*, 2010, **31**, 1025–1035.
43 I. Takeuchi, Y. Shimamura, Y. Kakami, T. Kameda, K. Hattori, S. Miura, H. Shirai, M. Okumura, T. Inagi, H. Terada and K. Makino, *Colloids Surf., B*, 2019, **175**, 564–568.
44 Q. Lu, H. Zhu, C. Zhang, F. Zhang, B. Zhang and D. L. Kaplan, *Biomacromolecules*, 2012, **13**, 826–832.
45 E. Wenk, A. J. Wandrey, H. P. Merkle and L. Meinel, *J. Controlled Release*, 2008, **132**, 26–34.
46 A. N. Mitropoulos, G. Perotto, S. Kim, B. Marelli, D. L. Kaplan and F. G. Omenetto, *Adv. Mater.*, 2014, **26**, 1105–1110.
47 C. Jiang, X. Wang, R. Gunawidjaja, Y. H. Lin, M. K. Gupta, D. L. Kaplan, R. R. Naik and V. V. Tsukruk, *Adv. Funct. Mater.*, 2007, **17**, 2229–2237.
48 D. Terada, Y. Yokoyama, S. Hattori, H. Kobayashi and Y. Tamada, *Mater. Sci. Eng. C*, 2016, **58**, 119–126.
49 Y. Qi, H. Wang, K. Wei, Y. Yang, R.-Y. Zheng, I. Kim and K.-Q. Zhang, *Int. J. Mol. Sci.*, 2017, **18**, 237.
50 Q. Lu, X. Hu, X. Wang, J. A. Kluge, S. Lu, P. Cebe and D. L. Kaplan, *Acta Biomater.*, 2010, **6**, 1380–1387.
51 J. E. Bressner, B. Marelli, G. Qin, L. E. Klinker, Y. Zhang, D. L. Kaplan and F. G. Omenetto, *J. Mater. Chem. B*, 2014, **2**, 4983–4987.
52 M. K. Gupta, S. Singamaneni, M. McConney, L. F. Drummy, R. R. Naik and V. V. Tsukruk, *Adv. Mater.*, 2010, **22**, 115–119.
53 N. E. Kurland, T. Dey, S. C. Kundu and V. K. J. A. M. Yadavalli, *Adv. Mater.*, 2013, **25**, 6207–6212.
54 H. Perry, A. Gopinath, D. L. Kaplan, L. Dal Negro and F. G. Omenetto, *Adv. Mater.*, 2008, **20**, 3070–3072.
55 J. J. Amsden, P. Domachuk, A. Gopinath, R. D. White, L. D. Negro, D. L. Kaplan and F. G. Omenetto, *Adv. Mater.*, 2010, **22**, 1746–1749.
56 J. A. Hunt, R. Chen, T. van Veen and N. Bryan, *J. Mater. Chem. B*, 2014, **2**, 5319–5338.
57 S. Kapoor and S. C. Kundu, *Acta Biomater.*, 2016, **31**, 17–32.

Open Access Article. Published on 08 September 2020. Downloaded on 1/22/2026 4:27:21 AM.
This article is licensed under a Creative Commons Attribution-NonCommercial 3.0 Unported Licence.

58 B. Galateanu, A. Hudita, C. Zaharia, M.-C. Bunea, E. Vasile, M.-R. Buga and M. Costache, *Polym. Polym. Compos., A Reference Series*, Springer, Cham, Switzerland, 2019, pp. 1791–1817.
59 J. L. Whittaker, R. Balu, R. Knott, L. de Campo, J. P. Mata, C. Rehm, A. J. Hill, N. K. Dutta and N. Roy Choudhury, *Int. J. Biol. Macromol.*, 2018, **114**, 998–1007.
60 Q. Lu, Y. Huang, M. Li, B. Zuo, S. Lu, J. Wang, H. Zhu and D. L. Kaplan, *Acta Biomater.*, 2011, **7**, 2394–2400.
61 A. L. Oliveira, L. Sun, H. J. Kim, X. Hu, W. Rice, J. Kluge, R. L. Reis and D. L. Kaplan, *Acta Biomater.*, 2012, **8**, 1530–1542.
62 P. Dorishetty, R. Balu, S. S. Athukoralalage, T. L. Greaves, J. Mata, L. de Campo, N. Saha, A. C. W. Zannettino, N. K. Dutta and N. R. Choudhury, *ACS Sustainable Chem. Eng.*, 2020, **8**, 2375–2389.
63 R. F. Pereira and P. J. Bártolo, *J. Appl. Polym. Sci.*, 2015, **132**, 42458.
64 J. L. Whittaker, N. R. Choudhury, N. K. Dutta and A. Zannettino, *J. Mater. Chem. B*, 2014, **2**, 6259–6270.
65 J. L. Whittaker, N. K. Dutta, A. Zannettino and N. R. Choudhury, *J. Mater. Chem. B*, 2016, **4**, 5519–5533.
66 R. Balu, S. Reeder, R. Knott, J. Mata, L. de Campo, N. K. Dutta and N. R. Choudhury, *Langmuir*, 2018, **34**, 9238–9251.
67 J. L. Whittaker, N. K. Dutta, C. M. Elvin and N. R. Choudhury, *J. Mater. Chem. B*, 2015, **3**, 6576–6579.
68 P. Dorishetty, R. Balu, A. Sreekumar, L. de Campo, J. P. Mata, N. R. Choudhury and N. K. Dutta, *ACS Sustainable Chem. Eng.*, 2019, **7**, 9257–9271.
69 S. Derakhshanfar, R. Mbeleck, K. Xu, X. Zhang, W. Zhong and M. Xing, *Bioact. Mater.*, 2018, **3**, 144–156.
70 M. J. Rodriguez, J. Brown, J. Giordano, S. J. Lin, F. G. Omenetto and D. L. Kaplan, *Biomaterials*, 2017, **117**, 105–115.
71 S. Ghosh, S. T. Parker, X. Wang, D. L. Kaplan and J. A. Lewis, *Adv. Funct. Mater.*, 2008, **18**, 1883–1889.
72 T. Dong, R. Mi, M. Wu, N. Zhong, X. Zhao, X. Chen and Z. Shao, *J. Mater. Chem. B*, 2019, **7**, 4328–4337.
73 S. H. Kim, Y. K. Yeon, J. M. Lee, J. R. Chao, Y. J. Lee, Y. B. Seo, M. T. Sultan, O. J. Lee, J. S. Lee, S.-i. Yoon, I.-S. Hong, G. Khang, S. J. Lee, J. J. Yoo and C. H. Park, *Nat. Commun.*, 2018, **9**, 1620.
74 M. Kazemimostaghim, R. Rjkhowa, T. Tsuzuki and X. Wang, *Powder Technol.*, 2013, **241**, 230–235.
75 T. Hino, M. Tanimoto and S. Shimabayashi, *J. Colloid Interface Sci.*, 2003, **266**, 68–73.
76 B. Kundu, R. Rajkhowa, S. C. Kundu and X. Wang, *Adv. Drug Delivery Rev.*, 2013, **65**, 457–470.
77 K. Y. Lee and D. J. Mooney, *Chem. Rev.*, 2001, **101**, 1869–1880.
78 C. Chung and J. A. Burdick, *Adv. Drug Delivery Rev.*, 2008, **60**, 243–262.
79 T. Franz, E. M. Hasler, R. Hagg, C. Weiler, R. P. Jakob and P. Mainil-Varlet, *Osteoarthr. Cartil.*, 2001, **9**, 582–592.
80 W. Zhu, V. C. Mow, T. J. Koob and D. R. Eyre, *J. Orthop. Res.*, 1993, **11**, 771–781.
81 B. Stemper, D. Board, N. Yoganandan and C. Wolfla, *J. Craniovertebral Junction Spine*, 2010, **1**, 18–22.
82 Y. Xia, K. I. Momot, Z. Chen, C. T. Chen, D. Kahn and F. Badar, *Introduction to Cartilage*, R. Soc. Chem., Cambridge, 2016, pp. 1–43.
83 M. J. Stoddart, S. Grad, D. Eglin and M. Alini, *Regen. Med.*, 2009, **4**, 81–98.
84 G. Cheng, Z. Davoudi, X. Xing, X. Yu, X. Cheng, Z. Li, H. Deng and Q. Wang, *ACS Biomater. Sci. Eng.*, 2018, **4**, 2704–2715.
85 K. Makaya, S. Terada, K. Ohgo and T. Asakura, *J. Biosci. Bioeng.*, 2009, **108**, 68–75.
86 S.-H. Park, E. S. Gil, B. B. Mandal, H. Cho, J. A. Kluge, B.-H. Min and D. L. Kaplan, *J. Tissue Eng. Regener. Med.*, 2012, **6**, s24–s33.
87 J. Hu, Y. Lu, L. Cai, K. G. Owusu-Ansah, G. Xu, F. Han, J. Bao, X. Lin and Y. Huang, *Sci. Rep.*, 2017, **7**, 2347.
88 H. Hong, Y. B. Seo, D. Y. Kim, J. S. Lee, Y. J. Lee, H. Lee, O. Ajiteru, M. T. Sultan, O. J. Lee, S. H. Kim and C. H. Park, *Biomaterials*, 2020, **232**, 119679.
89 Y. P. Singh, A. Bandyopadhyay and B. B. Mandal, *ACS Appl. Mater. Interfaces*, 2019, **11**, 33684–33696.
90 F. Zhou, X. Zhang, D. Cai, J. Li, Q. Mu, W. Zhang, S. Zhu, Y. Jiang, W. Shen, S. Zhang and H. W. Ouyang, *Acta Biomater.*, 2017, **63**, 64–75.
91 P. Bhattacharjee, B. Kundu, D. Naskar, H.-W. Kim, T. K. Maiti, D. Bhattacharya and S. C. Kundu, *Acta Biomater.*, 2017, **63**, 1–17.
92 Y. Cai, J. Guo, C. Chen, C. Yao, S.-M. Chung, J. Yao, I.-S. Lee and X. Kong, *Mater. Sci. Eng. C*, 2017, **70**, 148–154.
93 H.-J. Jin, J. Chen, V. Karageorgiou, G. H. Altman and D. L. Kaplan, *Biomaterials*, 2004, **25**, 1039–1047.
94 X. D. Kong, F. Z. Cui, X. M. Wang, M. Zhang and W. Zhang, *J. Cryst. Growth*, 2004, **270**, 197–202.
95 S. Bhumiratana, W. L. Grayson, A. Castaneda, D. N. Rockwood, E. S. Gil, D. L. Kaplan and G. Vunjak-Novakovic, *Biomaterials*, 2011, **32**, 2812–2820.
96 Y. Jin, B. Kundu, Y. Cai, S. C. Kundu and J. Yao, *Colloids Surf., B*, 2015, **134**, 339–345.
97 C. E. Schmidt and J. B. Leach, *Annu. Rev. Biomed. Eng.*, 2003, **5**, 293–347.
98 Q. Cao, R. L. Benton and S. R. Whittemore, *J. Neurosci. Res.*, 2002, **68**, 501–510.
99 A. M. Hopkins, L. De Laporte, F. Tortelli, E. Spedden, C. Staii, T. J. Atherton, J. A. Hubbell and D. L. Kaplan, *Adv. Funct. Mater.*, 2013, **23**, 5140–5149.
100 Y. Yang, X. Chen, F. Ding, P. Zhang, J. Liu and X. Gu, *Biomaterials*, 2007, **28**, 1643–1652.
101 A. Halim, Q. Luo, Y. Ju and G. Song, *Nanomaterials*, 2018, **8**, 736.
102 E. Afjeh-Dana, P. Naserzadeh, H. Nazari, F. Mottaghitalab, R. Shabani, N. Aminii, B. Mehravi, F. T. Rostami, M. T. Joghataei, K. Mousavizadeh and K. Ashtari, *Int. J. Biol. Macromol.*, 2019, **129**, 1034–1039.
103 M. Nune, S. Manchineella, T. Govindaraju and K. S. Narayana, *Mater. Sci. Eng. C*, 2019, **94**, 17–25.

 This journal is © The Royal Society of Chemistry 2020

Open Access Article. Published on 08 September 2020. Downloaded on 1/22/2026 4:27:21 AM.
This article is licensed under a Creative Commons Attribution-NonCommercial 3.0 Unported Licence.

104 S. Shrestha, B. K. Shrestha, J. Lee, O. K. Joong, B.-S. Kim, C. H. Park and C. S. Kim, *Mater. Sci. Eng. C*, 2019, **102**, 511–523.
105 C. R. Wittmer, T. Claudepierre, M. Reber, P. Wiedemann, J. A. Garlick, D. Kaplan and C. Egles, *Adv. Funct. Mater.*, 2011, **21**, 4232–4242.
106 C. D. Bostick, S. Mukhopadhyay, I. Pecht, M. Sheves, D. Cahen and D. Lederman, *Rep. Prog. Phys.*, 2018, **81**, 026601.
107 C. Wang, K. Xia, Y. Zhang and D. L. Kaplan, *Acc. Chem. Res.*, 2019, **52**, 2916–2927.
108 L.-D. Koh, J. Yeo, Y. Y. Lee, Q. Ong, M. Han and B. C. K. Tee, *Mater. Sci. Eng. C*, 2018, **86**, 151–172.
109 S. Y. Cho, Y. S. Yun, S. Lee, D. Jang, K.-Y. Park, J. K. Kim, B. H. Kim, K. Kang, D. L. Kaplan and H.-J. Jin, *Nat. Commun.*, 2015, **6**, 7145.
110 W.-H. Yeo, Y.-S. Kim, J. Lee, A. Ameen, L. Shi, M. Li, S. Wang, R. Ma, S. H. Jin, Z. Kang, Y. Huang and J. A. Rogers, *Adv. Mater.*, 2013, **25**, 2773–2778.
111 X. Wang, Y. Gu, Z. Xiong, Z. Cui and T. Zhang, *Adv. Mater.*, 2014, **26**, 1336–1342.
112 M. Zhang, C. Wang, Q. Wang, M. Jian and Y. Zhang, *ACS Appl. Mater. Interfaces*, 2016, **8**, 20894–20899.
113 B. Liang, L. Fang, Y. Hu, G. Yang, Q. Zhu and X. Ye, *Nanoscale*, 2014, **6**, 4264–4274.
114 Y. Luo, Y. Pei, X. Feng, H. Zhang, B. Lu and L. Wang, *Mater. Lett.*, 2020, **260**, 126945.
115 D.-L. Wen, X. Liu, H.-T. Deng, D.-H. Sun, H.-Y. Qian, J. Brugger and X.-S. Zhang, *Nano Energy*, 2019, **66**, 104123.
116 H. Tao, J. M. Kainerstorfer, S. M. Siebert, E. M. Pritchard, A. Sassaroli, B. J. Panilaitis, M. A. Brenckle, J. J. Amsden, J. Levitt and S. Fantini, *Proc. Natl. Acad. Sci. U. S. A.*, 2012, **109**, 19584–19589.
117 W. Burleson, S. S. Clark, B. Ransford and K. Fu, *Design Automation Conference*, 2012, pp. 12–17.
118 R. O. Darouiche, *N. Engl. J. Med.*, 2004, **350**, 1422–1429.
119 H. Tao, S.-W. Hwang, B. Marelli, B. An, J. E. Moreau, M. Yang, M. A. Brenckle, S. Kim, D. L. Kaplan and J. A. Rogers, *Proc. Natl. Acad. Sci. U. S. A.*, 2014, **111**, 17385–17389.
120 H. Tao, S. M. Siebert, M. A. Brenckle, R. D. Averitt, M. Cronin-Golomb, D. L. Kaplan and F. G. Omenetto, *Appl. Phys. Lett.*, 2010, **97**, 123702.
121 S. Hofmann, C. T. Wong Po Foo, F. Rossetti, M. Textor, G. Vunjak-Novakovic, D. L. Kaplan, H. P. Merkle and L. Meinel, *J. Controlled Release*, 2006, **111**, 219–227.
122 H. Yu, Z. Cui, P. Yu, C. Guo, B. Feng, T. Jiang, S. Wang, Q. Yin, D. Zhong, X. Yang, Z. Zhang and Y. Li, *Adv. Funct. Mater.*, 2015, **25**, 2489–2500.
123 P. Z. Elias, G. W. Liu, H. Wei, M. C. Jensen, P. J. Horner and S. H. Pun, *J. Controlled Release*, 2015, **208**, 76–84.
124 H. Wu, S. Liu, L. Xiao, X. Dong, Q. Lu and D. L. Kaplan, *ACS Appl. Mater. Interfaces*, 2016, **8**, 17118–17126.
125 W. K. Raja, S. MacCorkle, I. M. Diwan, A. Abdurrob, J. Lu, F. G. Omenetto and D. L. Kaplan, *Small*, 2013, **9**, 3704–3713.
126 S. Chen, H. Matsumoto, Y. Moro-oka, M. Tanaka, Y. Miyahara, T. Suganami and A. Matsumoto, *ACS Biomater. Sci. Eng.*, 2019, **5**, 5781–5789.
127 X. Wang, E. Wenk, X. Hu, G. R. Castro, L. Meinel, X. Wang, C. Li, H. Merkle and D. L. Kaplan, *Biomaterials*, 2007, **28**, 4161–4169.
128 X. Wang, X. Hu, A. Daley, O. Rabotyagova, P. Cebe and D. L. Kaplan, *J. Controlled Release*, 2007, **121**, 190–199.
129 X. Wang, H. J. Kim, P. Xu, A. Matsumoto and D. L. Kaplan, *Langmuir*, 2005, **21**, 11335–11341.
130 E. M. Pritchard and D. L. Kaplan, *Expet Opin. Drug Deliv.*, 2011, **8**, 797–811.
131 R. Elia, C. D. Michelson, A. L. Perera, T. F. Brunner, M. Harsono, G. G. Leisk, G. Kugel and D. L. Kaplan, *J. Biomed. Mater. Res., Part B*, 2015, **103**, 1602–1609.
132 H. Waizy, J.-M. Seitz, J. Reifenrath, A. Weizbauer, F.-W. Bach, A. Meyer-Lindenberg, B. Denkena and H. Windhagen, *J. Mater. Sci.*, 2013, **48**, 39–50.
133 G. Tullii, S. Donini, C. Bossio, F. Lodola, M. Pasini, E. Parisini, F. Galeotti and M. R. Antognazza, *ACS Appl. Mater. Interfaces*, 2020, **12**, 5437–5446.